Searching for Gluino LSP at the LHC

Essodjolo Kpatcha*a,b, Paulina Knees †c, Iñaki Lara‡d, Daniel E. López-Fogliani§c,e, Carlos Muñoz¶a,b, Natsumi Nagata¶f, and Hidetoshi Otono**g

^aDepartamento de Física Teórica, Universidad Autónoma de Madrid (UAM), Campus de Cantoblanco, 28049 Madrid, Spain

b Instituto de Física Teórica (IFT) UAM-CSIC, Campus de Cantoblanco, 28049 Madrid, Spain c Instituto de Física de Buenos Aires UBA & CONICET, Departamento de Física, Facultad de Ciencia Exactas y Naturales, Universidad de Buenos Aires, 1428 Buenos Aires, Argentina d Faculty of Physics, University of Warsaw, Pasteura 5, 02-093 Warsaw, Poland e Pontificia Universidad Católica Argentina, Av. Alicia Moreau de Justo 1500, 1107 Buenos Aires, Argentina

^fDepartment of Physics, University of Tokyo, Tokyo 113-0033, Japan ^gDepartment of Physics, Kyushu University, Fukuoka 819-0395, Japan

Abstract

We analyse relevant signals expected at the LHC, assuming that the gluino is the lightest supersymmetric particle (LSP) in the framework of the $\mu\nu$ SSM. In this R-parity violating model, the presence of couplings involving right-handed neutrinos solves simultaneously the μ problem and the accommodations of neutrino masses and mixing angles. We study gluino pair production in quark-antiquark and gluon-gluon collisions. The main decay channels for the gluino LSP are the three-body decays to two quarks and a lepton or a neutrino. In both cases, the leading channels occur for the third family of quarks. We compare the predictions of this scenario with LHC searches for prompt and long-lived particles. To analyse the parameter space we sample the $\mu\nu$ SSM for a gluino LSP, paying special attention to reproduce the current experimental data on neutrino and Higgs physics, as well as flavour observables. Our results imply a lower limit on the mass of the gluino LSP of about 2600 GeV, and an upper limit for the decay length of about 6 cm.

Keywords: Supersymmetry, R-parity violation, LHC signals, Gluino LSP.

^{*}kpatcha.essodjolo@uam.es

[†]pknees@df.uba.ar

[‡]inaki.lara@fuw.edu.pl

[§]daniel.lopez@df.uba.ar

[¶]c.munoz@uam.es

natsumi@hep-th.phys.s.u-tokyo.ac.jp

^{**}otono@phys.kyushu-u.ac.jp

Contents

1	Introduction	2
2	The $\mu\nu$ SSM	3
	2.1 The Neutrino Sector	5
	2.2 The Higgs Sector	6
	2.3 The Gluino Sector	7
3	Gluino LSP Phenomenology	7
	3.1 Decay Modes	8
	3.2 LHC Searches	9
4	Strategy for the Scanning	12
	4.1 Experimental Constraints	13
	4.2 Parameter Analysis	14
5	Results	17
6	Conclusions	18
\mathbf{A}	Validation of the Search for Displaced Leptons	20
В	Gluino LSP Relevant Interactions	22
	B.1 Gluino - down quark - down squark Interaction	22
	B.2 Gluino - up quark - up squark Interaction	23
	B.3 Up squark - down quark - lepton Interaction	23
	B.4 Down squark - up quark - lepton Interaction	24
	B.5 Up squark - up quark - neutrino Interaction	24
	B.6 Down squark - down quark - neutrino Interaction	25

1 Introduction

The ' μ from ν ' Supersymmetric Standard Model ($\mu\nu$ SSM) [1,2] (for a review, see Ref. [3]) is a predictive model alternative to the Minimal Supersymmetric Standard Model (MSSM) [4–8] and the Next-to-MSSM (NMSSM) [9,10]. In the $\mu\nu$ SSM, the presence of couplings involving right-handed (RH) neutrinos solves simultaneously the μ problem and the ν -problem (neutrino masses), without the need to introduce additional energy scales beyond the supersymmetry (SUSY)-breaking scale. In contrast to the MSSM, and the NMSSM, R-parity and lepton number are not conserved, leading to a completely different phenomenology characterized by distinct prompt or displaced decays of the lightest supersymmetric particle (LSP), producing multi-leptons/jets/photons with small/moderate missing transverse energy (MET) from neutrinos [11–18]. The smallness of neutrino masses is directly related with the low decay width of the LSP. Actually, it is also related to the existence of possible candidates for decaying dark matter in the model. This is the case of the gravitino [19–23], or the axino [24], with lifetimes greater than the age of the Universe. Recently, the role of sterile neutrinos as decaying dark matter candidates in the framework of the $\mu\nu$ SSM has

also being studied [25]. It is also worth mentioning, concerning cosmology, that baryon asymmetry might be realized in the $\mu\nu$ SSM through electroweak (EW) baryogenesis [26]. The EW sector of the $\mu\nu$ SSM can also explain [15,16] the longstanding discrepancy between the experimental result for the anomalous magnetic moment of the muon [27,28] and its SM prediction [29].¹

Because of R-parity violation (RPV) in the $\mu\nu$ SSM, basically all SUSY particles are candidates for the LSP, and therefore analyses of the LHC phenomenology associated to each candidate are necessary to test them. This crucial task, given the current experimental results on SUSY searches, has been mainly concentrated on the EW sector of the $\mu\nu$ SSM, analysing left sneutrinos, the right smuon and the bino as candidates for the LSP [11–16]. More recently, the colour sector of the $\mu\nu$ SSM has been analysed. In particular, in Ref. [17] the SUSY partners of the top quark as LSP candidates, i.e. the left and right stops, were considered, whereas in Ref. [18] the right sbottom was also considered. The aim of this work is to continue with the systematic analysis of the possible LSP's of the $\mu\nu$ SSM, focusing now on the gluino as the LSP.

Thus, we will study the constraints on the parameter space of the model by sampling it to get the gluino as the LSP in a wide range of masses. We will pay special attention to reproduce neutrino masses and mixing angles [30–35]. In addition, we will impose on the resulting parameters agreement with Higgs data as well as with flavour observables.

The paper is organized as follows. In Sec. 2, we will review the $\mu\nu$ SSM and its relevant parameters for our analysis of neutrino, neutral Higgs and gluino sectors. In Sec. 3, we will introduce the phenomenology of the gluino LSP, studying especially its signals at the LHC. They consist mainly of displaced vertices with two quarks and a lepton or a neutrino. In Sec. 4, we will discuss the strategy that we will employ to perform scans searching for points of the parameter space of our scenario compatible with current experimental data on neutrino and Higgs physics, as well as flavour observables such as B and μ decays. The results of these scans will be presented in Sec. 5, and applied to show the current reach of the LHC search on the parameter space of the gluino LSP based on ATLAS and CMS results [36–46]. Finally, our conclusions are left for Sec. 6.

2 The $\mu\nu$ SSM

In the $\mu\nu$ SSM [1–3], the particle content of the MSSM is extended by RH neutrino superfields $\hat{\nu}_i^c$. The simplest superpotential of the model is the following [1, 2, 11]:

$$W = \epsilon_{ab} \left(Y_{e_{ij}} \, \hat{H}_{d}^{a} \, \hat{L}_{i}^{b} \, \hat{e}_{j}^{c} + Y_{d_{ij}} \, \hat{H}_{d}^{a} \, \hat{Q}_{i}^{b} \, \hat{d}_{j}^{c} + Y_{u_{ij}} \, \hat{H}_{u}^{b} \, \hat{Q}^{a} \, \hat{u}_{j}^{c} \right)$$

$$+ \epsilon_{ab} \left(Y_{\nu_{ij}} \, \hat{H}_{u}^{b} \, \hat{L}_{i}^{a} \, \hat{\nu}_{j}^{c} - \lambda_{i} \, \hat{\nu}_{i}^{c} \, \hat{H}_{u}^{b} \hat{H}_{d}^{a} \right) + \frac{1}{3} \kappa_{ijk} \hat{\nu}_{i}^{c} \hat{\nu}_{j}^{c} \hat{\nu}_{k}^{c}, \qquad (1)$$

where the summation convention is implied on repeated indices, with i, j, k = 1, 2, 3 the usual family indices of the SM and a, b = 1, 2 $SU(2)_L$ indices with ϵ_{ab} the totally antisymmetric tensor, $\epsilon_{12} = 1$.

¹In this work we will not try to explain it, since we are interested in the analysis of a gluino LSP through the decoupling of the rest of the SUSY spectrum.

Working in the framework of a typical low-energy SUSY, the Lagrangian containing the soft SUSY-breaking terms related to W is given by:

$$-\mathcal{L}_{\text{soft}} = \epsilon_{ab} \left(T_{e_{ij}} H_d^a \widetilde{L}_{iL}^b \widetilde{e}_{jR}^* + T_{d_{ij}} H_d^a \widetilde{Q}_{iL}^b \widetilde{d}_{jR}^* + T_{u_{ij}} H_u^b \widetilde{Q}_{iL}^a \widetilde{u}_{jR}^* + \text{h.c.} \right)$$

$$+ \epsilon_{ab} \left(T_{\nu_{ij}} H_u^b \widetilde{L}_{iL}^a \widetilde{\nu}_{jR}^* - T_{\lambda_i} \widetilde{\nu}_{iR}^* H_d^a H_u^b + \frac{1}{3} T_{\kappa_{ijk}} \widetilde{\nu}_{iR}^* \widetilde{\nu}_{jR}^* \widetilde{\nu}_{kR}^* + \text{h.c.} \right)$$

$$+ m_{\widetilde{Q}_{ijL}}^2 \widetilde{Q}_{iL}^a \widetilde{Q}_{jL}^a + m_{\widetilde{u}_{ijR}}^2 \widetilde{u}_{iR}^* \widetilde{u}_{jR} + m_{\widetilde{d}_{ijR}}^2 \widetilde{d}_{iR}^* \widetilde{d}_{jR} + m_{\widetilde{L}_{ijL}}^2 \widetilde{L}_{iL}^a \widetilde{L}_{jL}^a$$

$$+ m_{\widetilde{\nu}_{ijR}}^2 \widetilde{\nu}_{iR}^* \widetilde{\nu}_{jR} + m_{\widetilde{e}_{ijR}}^2 \widetilde{e}_{iR}^* \widetilde{e}_{jR} + m_{H_d}^2 H_d^a * H_d^a + m_{H_u}^2 H_u^a * H_u^a$$

$$+ \frac{1}{2} \left(M_3 \widetilde{g} \widetilde{g} + M_2 \widetilde{W} \widetilde{W} + M_1 \widetilde{B}^0 \widetilde{B}^0 + \text{h.c.} \right).$$

$$(2)$$

In the early universe, not only the EW symmetry is broken, but in addition to the neutral components of the Higgs doublet fields H_d and H_u also the left and right sneutrinos $\tilde{\nu}_{iL}$ and $\tilde{\nu}_{iR}$ acquire a vacuum expectation value (VEV). With the choice of CP conservation, they develop real VEVs denoted by:

$$\langle H_d^0 \rangle = \frac{v_d}{\sqrt{2}}, \quad \langle H_u^0 \rangle = \frac{v_u}{\sqrt{2}}, \quad \langle \widetilde{\nu}_{iR} \rangle = \frac{v_{iR}}{\sqrt{2}}, \quad \langle \widetilde{\nu}_{iL} \rangle = \frac{v_{iL}}{\sqrt{2}}.$$
 (3)

The EW symmetry breaking is induced by the soft SUSY-breaking terms producing $v_{iR} \sim \mathcal{O}(1 \text{ TeV})$ as a consequence of the right sneutrino minimization equations in the scalar potential [1, 2, 11]. Since $\tilde{\nu}_{iR}$ are gauge-singlet fields, the μ -problem can be solved in total analogy to the NMSSM through the presence in the superpotential (1) of the trilinear terms $\lambda_i \, \hat{\nu}_i^c \, \hat{H}_u \hat{H}_d$. Then, the value of the effective μ -parameter is given by $\mu = \lambda_i v_{iR} / \sqrt{2}$. These trilinear terms also relate the origin of the μ -term to the origin of neutrino masses and mixing angles, since neutrino Yukawa couplings $Y_{\nu_{ij}} \hat{H}_u \, \hat{L}_i \, \hat{\nu}_j^c$ are present in the superpotential generating Dirac masses for neutrinos, $m_{\mathcal{D}_{ij}} \equiv Y_{\nu_{ij}} v_u / \sqrt{2}$. Remarkably, in the $\mu\nu$ SSM it is possible to accommodate neutrino masses and mixing in agreement with experiments [30–35] via an EW seesaw mechanism dynamically generated during the EW symmetry breaking [1, 2, 47–51]. The latter takes place through the couplings $\kappa_{ijk}\hat{\nu}_i^c\hat{\nu}_j^c\hat{\nu}_k^c$, giving rise to effective Majorana masses for RH neutrinos $\mathcal{M}_{ij} = 2\kappa_{ijk}v_{kR}/\sqrt{2}$. Actually, this is possible at tree level even with diagonal Yukawa couplings [47, 49]. It is worth noticing here that the neutrino Yukawas discussed above also generate the effective bilinear terms $\mu_i \hat{H}_u \, \hat{L}_i$ with $\mu_i = Y_{\nu_{ij}} v_{iR}/\sqrt{2}$, used in the bilinear RPV model (BRPV) [52].

We conclude, therefore, that the $\mu\nu$ SSM solves not only the μ -problem, but also the ν -problem, without the need to introduce energy scales beyond the SUSY-breaking one.

The parameter space of the $\mu\nu$ SSM, and in particular the neutrino, neutral Higgs and gluino sectors are relevant for our analysis in order to reproduce neutrino and Higgs data, and to obtain in the spectrum a gluino as the LSP. In particular, neutrino and Higgs sectors were discussed in Refs. [14, 53, 15, 16], and we refer the reader to those works for details, although we will summarize the results below. First, we discuss here several simplifications that are convenient to take into account given the large number of parameters of the model. Using diagonal mass matrices for the scalar fermions, in order to avoid the strong upper bounds upon the intergenerational scalar mixing (see e.g. Ref. [54]), from the eight minimization conditions with respect to v_d , v_u , v_{iR} and v_i to facilitate the computation we

prefer to eliminate the soft masses $m_{H_d}^2$, $m_{H_u}^2$, $m_{\tilde{\nu}_{iR}}^2$ and $m_{\tilde{L}_{iL}}^2$ in favour of the VEVs. Also, we assume for simplicity in what follows the flavour-independent couplings and VEVs $\lambda_i = \lambda$, $\kappa_{ijk} = \kappa \delta_{ij} \delta_{jk}$, and $v_{iR} = v_R$. Then, the Higgsino mass parameter μ , bilinear couplings μ_i and Dirac and Majorana masses discussed above are given by:

$$\mu = 3\lambda \frac{v_R}{\sqrt{2}}, \quad \mu_i = Y_{\nu_i} \frac{v_R}{\sqrt{2}}, \quad m_{\mathcal{D}_i} = Y_{\nu_i} \frac{v_u}{\sqrt{2}}, \quad \mathcal{M} = 2\kappa \frac{v_R}{\sqrt{2}},$$
 (4)

where we have already used the possibility of having diagonal neutrino Yukawa couplings $Y_{\nu_{ij}} = Y_{\nu_i} \delta_{ij}$ in the $\mu \nu SSM$ in order to reproduce neutrino physics.

2.1 The Neutrino Sector

For light neutrinos, under the above assumptions, one can obtain the following simplified formula for the effective mass matrix [49]:

$$(m_{\nu})_{ij} \approx \frac{m_{\mathcal{D}_i} m_{\mathcal{D}_j}}{3\mathcal{M}} (1 - 3\delta_{ij}) - \frac{v_{iL} v_{jL}}{4M}, \qquad \frac{1}{M} \equiv \frac{g^{\prime 2}}{M_1} + \frac{g^2}{M_2},$$
 (5)

where g', g are the EW gauge couplings, and M_1 , M_2 the bino and wino soft SUSY-breaking masses, respectively. This expression arises from the generalized EW seesaw of the $\mu\nu$ SSM, where due to RPV the neutral fermions have the flavour composition $(\nu_{iL}, \widetilde{B}^0, \widetilde{W}^0, \widetilde{H}_d^0, \widetilde{H}_u^0, \nu_{iR})$. The first two terms in Eq. (5) are generated through the mixing of ν_{iL} with ν_{iR} -Higgsinos, and the third one also include the mixing with the gauginos. These are the so-called ν_R -Higgsino seesaw and gaugino seesaw, respectively [49]. One can see from this equation that once \mathcal{M} is fixed, as will be done in the parameter analysis of Sec. 4.2, the most crucial independent parameters determining neutrino physics are:

$$Y_{\nu_i}, v_{iL}, M_1, M_2.$$
 (6)

Note that this EW scale seesaw implies $Y_{\nu_i} \lesssim 10^{-6}$ driving v_{iL} to small values because of the proportional contributions to Y_{ν_i} appearing in their minimization equations. A rough estimation gives $v_{iL} \lesssim m_{\mathcal{D}_i} \lesssim 10^{-4}$.

Considering the normal ordering for the neutrino mass spectrum, and taking advantage of the dominance of the gaugino seesaw for some of the three neutrino families, three representative type of solutions for neutrino physics using diagonal neutrino Yukawas were obtained in Ref. [14]. In our analysis we will use the so-called type 2 solutions, which have the structure

$$M > 0$$
, with $Y_{\nu_3} < Y_{\nu_1} < Y_{\nu_2}$, and $v_{1L} < v_{2L} \sim v_{3L}$, (7)

In this case of type 2, it is easy to find solutions with the gaugino seesaw as the dominant one for the third family. Then, v_{3L} determines the corresponding neutrino mass and Y_{ν_3} can be small. On the other hand, the normal ordering for neutrinos determines that the first family dominates the lightest mass eigenstate implying that $Y_{\nu_1} < Y_{\nu_2}$ and $v_{1L} < v_{2L}, v_{3L}$, with both ν_R -Higgsino and gaugino seesaws contributing significantly to the masses of the first and second family. Taking also into account that the composition of the second and third families in the second mass eigenstate is similar, we expect $v_{2L} \sim v_{3L}$. In Ref. [14],

a quantitative analysis of the neutrino sector was carried out, with the result that the hierarchy qualitatively discussed above for Yukawas and VEVs works properly. See in particular Fig. 4 of Ref. [14], where $\delta m^2 = m_2^2 - m_1^2$ versus Y_{ν_i} and v_{iL} is shown for the scans carried out in that work, using the results for normal ordering from Ref. [35].

We will argue in Sec. 5 that the other two type of solutions of normal ordering for neutrino physics are not going to modify our results. The same conclusion is obtained in the case of working with the inverted ordering for the neutrino mass spectrum. The structure of the solutions is more involved for this case, because the two heaviest eigenstates are close in mass and the lightest of them has a dominant contribution from the first family. Thus, to choose Y_{ν_1} as the largest of the neutrino Yukawas helps to satisfy these relations. For the second and third family, a delicate balance between the contributions of ν_R -Higgsino and gaugino seesaws is needed in order to obtain the correct mixing angles. In particular, a representative type of solutions for the case of inverted ordering has the structure M > 0, with $Y_{\nu_3} \sim Y_{\nu_2} < Y_{\nu_1}$, and $v_{1L} < v_{2L} \sim v_{3L}$.

2.2 The Higgs Sector

The neutral Higgses are mixed with right and left sneutrinos, since the neutral scalars and pseudoscalars in the $\mu\nu$ SSM have the flavour composition $(H_d^0, H_u^0, \tilde{\nu}_{iR}, \tilde{\nu}_{iL})$. Nevertheless, the left sneutrinos are basically decoupled from the other states, since the off-diagonal terms of the mass matrix are suppressed by the small $Y_{\nu_{ij}}$ and v_{iL} . Unlike the latter states, the other neutral scalars can be substantially mixed. Neglecting this mixing between the doublet-like Higgses and the three right sneutrinos, the expression of the tree-level mass of the SM-like Higgs is [2]:

$$m_h^2 \approx m_Z^2 \left(\cos^2 2\beta + 10.9 \,\lambda^2 \sin^2 2\beta\right),\tag{8}$$

where $\tan \beta = v_u/v_d$, and m_Z denotes the mass of the Z boson. Effects lowering (raising) this mass appear when the SM-like Higgs mixes with heavier (lighter) right sneutrinos. The one-loop corrections are basically determined by the third-generation soft SUSY-breaking parameters $m_{\widetilde{u}_{3R}}$, $m_{\widetilde{Q}_{3L}}$ and T_{u_3} (where we have assumed for simplicity that for all soft trilinear parameters $T_{ij} = T_i \delta_{ij}$). These three parameters, together with the coupling λ and $\tan \beta$, are the crucial ones for Higgs physics. Their values can ensure that the model contains a scalar boson with a mass around ~ 125 GeV and properties similar to the ones of the SM Higgs boson [55, 56, 53, 57].

In addition, κ , v_R and the trilinear parameter T_{κ} in the soft Lagrangian (2), are the key ingredients to determine the mass scale of the right sneutrinos [2,47]. For example, for $\lambda \lesssim 0.01$ they are basically free from any doublet admixture, and using their minimization equations in the scalar potential the scalar and pseudoscalar masses can be approximated respectively by [58,11]:

$$m_{\widetilde{\nu}_{iR}}^2 \approx \frac{v_R}{\sqrt{2}} \left(T_\kappa + \frac{v_R}{\sqrt{2}} 4\kappa^2 \right), \quad m_{\widetilde{\nu}_{iR}}^2 \approx -\frac{v_R}{\sqrt{2}} 3T_\kappa.$$
 (9)

Finally, λ and the trilinear parameter T_{λ} not only contribute to these masses for larger values of λ , but also control the mixing between the singlet and the doublet states and hence, they contribute in determining their mass scales as discussed in detail in Ref. [53].

We conclude that the relevant parameters in the Higgs (-right sneutrino) sector are:

$$\lambda, \kappa, \tan \beta, v_R, T_{\kappa}, T_{\lambda}, T_{u_3}, m_{\widetilde{u}_{3R}}, m_{\widetilde{Q}_{3L}}.$$
 (10)

Note that the most crucial parameters for the neutrino sector (6) are basically decoupled from these parameters controlling Higgs physics. This simplifies the analysis of the parameter space of the model, as will be discussed in Sec. 4.2.

2.3 The Gluino Sector

The gluino sector of the $\mu\nu$ SSM coincide with that of the MSSM. Gluinos are the fermionic superpartners of the gluons and, therefore, carry colour charge, thus participating in strong interactions. The gluino mass $m_{\tilde{g}}$ arises from the soft SUSY-breaking terms, being essentially determined by the soft mass parameter M_3 , and further influenced by loop corrections. In this work, we will take M_3 to be a low-energy free parameter, compute $m_{\tilde{g}}$ taking into account the one loop corrections, and discuss the limits on it from available experimental data.

In our analysis of Sec. 5., we will sample the relevant parameter space of the $\mu\nu$ SSM, which contains the independent parameters determining neutrino and Higgs physics in Eqs. (6) and (10). Nevertheless, the parameters for neutrino physics Y_{ν_i} , v_{iL} , M_1 and M_2 are essentially decoupled from the parameters controlling Higgs physics, as already mentioned. Thus, for a suitable choice of the former parameters reproducing neutrino physics, there is still enough freedom to reproduce in addition Higgs data by playing with λ , κ , v_R , $\tan \beta$, T_{u_3} , etc., as shown in Refs. [14–16]. As a consequence, we will not need to scan over most of the latter parameters, relaxing our computing task. For this task we have employed the Multinest [59] algorithm as optimizer. To compute the spectrum and the observables we have used SARAH [60] to generate a SPheno [61,62] version for the model.

3 Gluino LSP Phenomenology

Gluinos can be abundantly produced at the LHC (see Refs. [63,64]). Since they interact only via strong interactions, they can be generated in pairs through quark-antiquark and gluon-gluon collisions, or singly in association with squarks. Gluino-squark associated production can be important for constraining scenarios of nearly degenerate gluinos and squarks, specially for full degeneracy in the squark sector. However, the points studied in the present work have mass differences between the gluino and the lightest squark in the range of hundreds of GeV, therefore the gluino-squark production is subleading with respect to gluino pair production. Then, we considered pair production as our case of interest, and the cross-sections used for this analysis in Sec. 3.2 were obtained at NNLO+NNLL using NNLL-fast [65]. In particular, for our range of interest of gluino masses between 500 GeV and 3000 GeV, the production cross-section is in the range between ~ 33.5 pb and 6×10^{-6} pb.

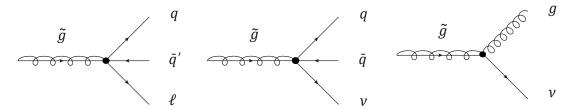


Figure 1: Relevant decay channels in the $\mu\nu$ SSM for a gluino LSP. (left) Decay to quark-antiquark and lepton; (centre) Decay to quark-antiquark and neutrino; (right) Decay to gluon and neutrino.

3.1 Decay Modes

Gluino decays to Standard Model particles have been discussed in the framework of the MSSM (see, e.g., Refs. [66,67]). In the $\mu\nu$ SSM, there are three relevant decay modes of the gluino LSP. On the one hand, the gluino has two three-body decays to two quarks and a lepton or a neutrino, mediated by virtual squarks. These are shown in Fig 1 left and centre. On the other hand, the gluino can decay to gluon and neutrino through a virtual quark-squark loop. This channel is shown in Fig 1 right. However, given the large values of the gluino masses analysed, this channel is subleading compared to the three-body decays.

The relevant interactions for the two dominant channels are then given in Appendix B. The gluino decays to a quark and a virtual squark, which subsequently decays to another quark and a lepton or a neutrino. Thus, gluino-quark-squark interactions are shown in (B.1) and (B.2), whereas squark-quark-lepton/neutrino interactions are shown in (B.3)-(B.6).

In the latter interactions, one can identify the most important contributions for the squark decays. There, U^V is the matrix which diagonalizes the mass matrix for the neutral fermions. The entries U^V_{i4} , U^V_{i5} and U^V_{i6} , correspond to the mixing between neutrinos and bino, winos and neutral Higgsino \widetilde{H}^0_d , respectively. They can be approximated as

$$U_{i4}^{V} \approx \frac{-g'}{M_1} \sum_{l} \frac{v_{lL}}{\sqrt{2}} U_{il}^{\text{PMNS}}, \qquad U_{i5}^{V} \approx \frac{g}{M_2} \sum_{l} \frac{v_{lL}}{\sqrt{2}} U_{il}^{\text{PMNS}}, \qquad U_{i6}^{V} \approx \frac{1}{\mu} \sum_{l} \frac{\mu_l}{\sqrt{2}} U_{il}^{\text{PMNS}}, \quad (11)$$

where U_{il}^{PMNS} are the entries of the PMNS matrix, with i and l neutrino physical and flavour indices, respectively. We also approximate other entries of the matrices involved in the computation, as follows: $U_{L,i4}^e \approx 0$ (vanishing charged wino-lepton mixing), $U_{R,i4}^e \approx gv_{iL}/M_2\sqrt{2}$, $U_{i7}^V \approx 0$ (vanishing neutrino-Higgsino \widetilde{H}_u^0 mixing), $U_{L,j5}^e \approx Y_{e_i}v_{iL}/\sqrt{2}\mu$.

Then, on the one hand, there are contributions of a squark decaying to quark and lepton corresponding to the term multiplying the projector P_L and the second term multiplying the projector P_R in both (B.3) and (B.4). Thus, they occur mainly through the Yukawa couplings $Y_{t,b}$ of \tilde{t} (\tilde{b}) with b (t) and charged Higgsinos, via the mixing between the latter and ℓ . In addition, there is the contribution of the first term multiplying the projector P_R in (B.4), which occurs through the gauge coupling t0 of t1 with t2 and charged winos, via the mixing between the latter and t2. On the other hand, there are contributions of a squark decaying to quark and neutrino corresponding to the first term multiplying the projector t2 and the second and third terms multiplying the projector t3 in both (B.5) and (B.6). They occur through the gauge couplings t3 and t4 of t3 with t4 (t4 and neutral winos and

binos, via the mixing between the latter and ν . In addition, there are the contributions of the first term multiplying the projector P_R and the second term multiplying the projector P_L in (B.6), which occur through the Yukawa coupling Y_b of \tilde{b} with b and neutral Higgsinos, via the mixing between the latter and ν . The contributions occurring through the Yukawa coupling Y_t of \tilde{t} with t and neutral Higgsinos \tilde{H}^0_u in (B.5), via the mixing between the latter and ν , are neglected below in Eq. (12) because such a mixing is very small, $U^V_{i7} \approx 0$, as discussed above.

Assuming pure squark states with a common mass fixed at $m_{\tilde{q}}$, and taking into account the above approximations, the values of the partial decay widths of the gluino LSP can be written as:

$$\sum_{i} \Gamma(\widetilde{g} \to t\bar{t}\nu_{i}) \sim \frac{g_{s}^{2}}{3072\pi^{3}} \frac{m_{\widetilde{g}}^{5}}{m_{\widetilde{q}}^{4}} \sum_{i} \left(\frac{1}{2} g^{2} U_{i5}^{V^{2}} + \frac{17}{18} g'^{2} U_{i4}^{V^{2}} + \frac{gg'}{3} U_{i5}^{V} U_{i4}^{V} \right), \tag{12}$$

$$\sum_{i,a\neq t} \Gamma(\widetilde{g} \to q\bar{q}\nu_i) \sim \frac{g_s^2}{3072\pi^3} \frac{m_{\widetilde{g}}^5}{m_{\widetilde{q}}^4} \sum_i \left(\frac{5}{2} g^2 U_{i5}^{V^2} + \frac{49}{18} g'^2 U_{i4}^{V^2} - \frac{gg'}{3} U_{i5}^V U_{i4}^V + Y_b^2 U_{i6}^{V^2} \right) (13)$$

$$\Gamma(\tilde{g} \to t\bar{b}\ell_i^-) = \Gamma(\tilde{g} \to \bar{t}b\bar{\ell}_i^+) \sim \frac{g_s^2}{3072\pi^3} \frac{m_{\tilde{g}}^5}{m_{\tilde{q}}^4} \left(\frac{g^4}{M_2^2} \frac{v_{iL}^2}{2} + \frac{Y_t^2 Y_{e_i}^2 v_{iL}^2}{\mu^2} + \frac{2Y_b^2 \mu_i^2}{\mu^2} \right), (14)$$

$$\sum_{g \neq t} \Gamma(\tilde{g} \to q\bar{q}'\ell_i^-) = \sum_{g \neq t} \Gamma(\tilde{g} \to q'\bar{q}\bar{\ell}_i^+) \sim \frac{g_s^2 g^2}{3072\pi^3} \frac{m_{\tilde{g}}^5}{m_{\tilde{q}}^4} \left(\frac{2g^4}{M_2^2} \frac{v_{iL}^2}{2}\right), \tag{15}$$

$$\sum_{i} \Gamma(\tilde{g} \to g\nu_{i}) \sim \frac{g_{s}^{4} Y_{t}^{2} \sum_{i} U_{i4}^{V}}{2048\pi^{5}} \frac{m_{t}^{2} m_{\tilde{g}}^{3}}{m_{\tilde{q}}^{4}} \left(1 + \log \frac{m_{t}^{2}}{m_{\tilde{q}}^{2}}\right)^{2}, \tag{16}$$

where in Eq. (14) the summation convention on repeated indices does not apply in the second term. Let us remark nevertheless that the results of Sec. 5 have been obtained using the full tree-level numerical computation of decay widths implemented in SPheno.

As can be deduced from these equations, when the quarks in the final state belong to the third family, the decay width becomes more relevant because of the contributions of bottom and top Yukawa couplings in Eqs. (13) and (14). The exception is the $\tilde{g} \to t\bar{t}\nu_i$ channel, since the contribution of the top Yukawa coupling is negligible, as discussed above.

3.2 LHC Searches

The gluino LSP would produce a diverse phenomenology at the LHC, as shown as in Fig. 1. The possible decays include: the production of a lepton $(e, \mu \text{ or } \tau)/\text{neutrino}$ and 2 quarks (including bottom and top quarks) or the production of a neutrino and a gluino. Consequently, the production of a pair of gluinos will lead to events that can include missing energy, leptons, several jets and b-jets. In addition, the decay length of the gluino LSP ranges from mm scale up to ~ 100 m. Therefore, different LHC searches will have the highest sensitivity for each case. We will classify the signals according to the lifetime scale and the LHC detection strategy. All constraints will be finally applied to each point analysed.

Case i) Large ionization energy loss

Whenever the gluino LSP is long-lived enough to measure ionization energy loss and/or time of flight, the searches for heavy charged long-lived particles are able to put strong constraints which are independent of the decay of the gluino LSP. In particular, for each point of the parameter space with a gluino LSP with proper lifetime greater than 3 m, the ATLAS search for heavy charged long-lived particles excludes gluino masses below 2200 GeV [36,37]. For each point tested, we exclude it if the mass of the gluino LSP is below the exclusion limit obtained by the ATLAS search for the specific value of $c\tau$.

Case ii) Non-prompt jets

The timing capabilities of the CMS electromagnetic calorimeter allow discriminating jets arriving at times significantly larger than the travelling times expected for light hadrons, which are moving at velocities close to the speed of light. This time delay can be associated with two effects: First, the larger indirect path formed by the initial trajectory of a long-lived particle plus the subsequent trajectories of the child particles. Secondly, the slower velocity of the long-lived particle due to the high mass compared to light hadrons. Such analysis is performed by the CMS collaboration in the work [38] in the context of long-lived gluinos decaying to gluons and stable gravitinos, excluding gluinos with masses of ~ 2500 GeV for lifetimes of ~ 1 m.

The case where the gluino LSP decays producing a neutrino and a gluon with proper decay lengths above ~ 30 cm will produce the same signal as the one analysed in [38]. For each point tested in this search, we compare the 95% observed upper limit on cross-section corresponding to events containing a delayed jet for a given parent particle mass and $c\tau$, with the prediction of the signal cross-section calculated as $\sigma(pp \to \tilde{g}\tilde{g}) \times [BR(\tilde{g} \to g\nu)^2 + 2BR(\tilde{g} \to g\nu)(1 - BR(\tilde{g} \to g\nu))]$.

Case iii) Displaced vertices

For shorter lifetimes, one can confront the points of the model with the limits from events with displaced vertices, including jets. The ATLAS search [39] targets final states with at least one displaced vertex (DV) with a high reconstructed mass and a large track multiplicity in events with large missing transverse momentum. It searches in particular for the signal of long-lived gluinos decaying as $\tilde{g} \to \bar{q}q\tilde{\chi}^0$. The CMS search [40] also searches for long-lived gluinos decaying into various final-state topologies containing displaced jets. In particular, it searches for the characteristic signals of long-lived gluino pair production decaying as $\tilde{g} \to g\tilde{\chi}^0$ or $\tilde{g} \to \bar{q}q\tilde{\chi}^0$.

These searches originally target long-lived massive particles with lifetimes in the range 1-10000 mm. Thus, this search can be sensitive to the gluino LSP when $c\tau$ is in this range. Some of the signal topologies analysed in the search match exactly the ones originated from the decays shown in Fig. 1. The case where the gluino LSP decays producing a neutrino and a gluon, or a pair of quarks and a neutrino, with proper decay lengths above ~ 1 mm is contrasted with the model-dependent limits obtained in the ATLAS and CMS searches for displaced vertices. For each point, we compare the 95% observed upper limit on cross-section with the prediction of the signal cross-section calculated in our model, similarly to Case (ii).

The CMS search [46] targets similar topologies and proper decay lengths as does [40], but

using a machine learning algorithm to improve the background rejection power. However, the limits obtained for the topologies studied here are equivalent in both searches, thus no improved limit can be obtained for the gluino LSP from this analysis.

There are other decay channels of the gluino LSP that can produce displaced vertices but do not match exactly the topologies explored in the searches [39,40]. To have a reasonable estimate of the exclusion power of those searches over the additional signals, we use a recast version of the ATLAS analysis within CheckMATE-LLP [68]. CheckMATE [69,70] is a universal tool for the recasting of LHC searches in the context of arbitrary new physics models. It uses the fast detector simulation framework Delphes [71] with customized AT-LAS detector card and additional built-in tuning for a more accurate reproduction of experimental efficiencies. The validation of the recast search is discussed in [68]. We generate signal Monte Carlo (MC) samples of gluino pair production with MadGraph5 aMC@NLOv3.4.2 [72–74] at leading order (LO). The hard event corresponds to tree-level production of gluino pairs and includes the emission of up to two additional partons, the NNPDF23LO [75, 76] PDF set is used. Simulated signal events were passed to Pythia-8.306 [77] for parton showering (PS) and hadronization. Jet matching and merging to parton-shower calculations is accomplished by the MLM algorithm [78]. Gluino pair-production nominal cross-sections are derived at NNLO+NNLL using NNLL-fast-3.0 [65, 79–81]. Finally, we process the events generated through CheckMATE. The results are used to calculate the efficiency (ϵ) of the search, defined as the number of events predicted in the signal region divided by the total number of generated events.

We generate samples for values of the mass equal to [2000, 2250, 2500, 2750] GeV, $c\tau$ equal to [1, 2, 5, 10, 20, 50, 100, 200, 500] mm and for all the different combinations of decays shown in Fig. 1, and calculate ϵ for each case. For each point tested in this work, we calculate the ϵ interpolating from each channel and value of mass and $c\tau$, within the set of ϵ obtained as described above.

Finally, the point is considered excluded if the total number of events predicted in the signal region of the search [39], calculated as the sum of $\mathcal{L} \times \sigma(pp \to \tilde{g}\tilde{g}) \times BR_{channel} \times \epsilon_{channel}$ over all channels, is greater than the 95% upper limit on signal events, which correspond to approximately 3 events.

Case iv) Displaced jets+muon

The ATLAS search for long-lived massive particles in events with a DV and a muon with large impact parameter [41], is designed to look for long-lived stops decaying to a quark and a muon. A similar event topology is possible when the gluino LSP decays producing two quarks and a muon, but in this case producing a vertex with a muon and two jets instead of one. Since there is no explicit restriction in the upper number of tracks matched to the secondary vertex, there is no reason to consider that the additional jet will spoil the efficiency of the search. On the contrary, the requirements on the full DV selection of $n_{tracks}^{DV} > 3$ and $m_{DV} > 20$ GeV will be easier to satisfy with increased hadronic activity associated to the DV.

For each point, we compare the 95% observed upper limit on cross-section, corresponding to the signal of one DV and one displaced muon originated from the decay of two long-lived stops for a given mass and $c\tau$, with the prediction of the signal cross-section calculated as $\sigma(pp \to \tilde{g}\tilde{g}) \times BR(\tilde{g} \to \bar{q}q'\mu)^2$.

Case v) Displaced leptons

The gluino LSP can decay producing leptons directly when it decays as $\tilde{g} \to \bar{q}q'l$ as shown in Fig. 1, or in the decay of a top quark when any of the quarks produced is a top quark. The ATLAS search for displaced leptons [42] looks for events with at least two leptonic tracks with an impact parameter greater than 3 mm and, as no requirements were made on missing energy, displaced vertices, or jets, the limits are applicable in general to any BSM model producing high- p_T displaced leptons.

Following a similar procedure to the case of DVs, we recast the analysis within CheckMATE-LLP. The validation of the recast search is discussed in Appendix A. We calculate the ϵ of the search, following the procedure described for the case of DVs, for the same set of masses and proper decay lengths. For each point tested, we calculate the ϵ interpolating from each channel and value of mass and $c\tau$, within the set of ϵ obtained as described above.

Finally, the point is considered excluded if the total number of events predicted in the signal region of the search [42], calculated as the sum of $\mathcal{L} \times \sigma(pp \to \tilde{g}\tilde{g}) \times BR_{channel} \times \epsilon_{channel}$ over all channels, is greater than the 95% upper limit on signal events, which correspond to 3 events.

Case vi) Prompt decays

Whenever the proper decay length of the gluino LSP is sufficiently small, $c\tau \lesssim 0.5$ mm, the limits calculated for the gluino decaying immediately after production will be sensitive to the gluino LSP. In particular, the ATLAS search [43] looks for gluinos decaying as $\tilde{g} \to \bar{q}q\bar{q}q\nu/l$ through the $\lambda'\bar{L}Qd$ R-parity violating coupling. A similar signal is obtained for the gluino LSP from the diagrams in Fig. 1 (left and centre). We constrain the points analysed in this search with $c\tau \lesssim 0.5$ mm the 95% observed upper limit on cross-section, corresponding to the signal of two gluinos decaying as $\tilde{g} \to \bar{q}q\bar{q}q\nu/l$, for massless neutralinos, with the prediction of the signal cross-section calculated as $\sigma(pp \to \tilde{g}\tilde{g}) \times BR(\tilde{g} \to \bar{q}q\nu/l)^2$.

The ATLAS search [44] target some of the signals constrained in [43] but the former is optimized for signals including at least tree leptons or two same-sign leptons while the latter is optimized for signals with a single isolated lepton. The search [44] impose constraints over the signal topology described in this section, however the limits obtained are equivalent to the ones obtained in [43], therefore is not possible to use this search to strengthen the limits over the gluino LSP.

Finally, The CMS search [45] uses a Deep-Neural-Network based tagger to discriminate decays of long-lived particles including jets and missing transverse momentum over a large range of $c\tau$. The search is optimized to constrain the decay of NLSP neutralino to a gravitino and either a Higgs boson or a Z boson, producing a final signal similar to the one in Fig. 1 left. However, the more stringent limit over the signal cross-section obtained is 0.8 fb which is larger than the production cross-section corresponding to the lightest allowed gluino LSP.

4 Strategy for the Scanning

In this section, we describe the methodology that we have employed to search for points in our parameter space that are compatible with the current experimental data on neutrino and Higgs physics, as well as ensuring that the gluino is the LSP. In addition, we have demanded the compatibility with some flavour observables, such as B and μ decays. To this end, we have performed scans on the parameter space of the model, with the input parameters optimally chosen.

4.1 Experimental Constraints

All experimental constraints (except the LHC searches, which are discussed in the previous section) are taken into account as follows:

• Neutrino observables

We have imposed the results for normal ordering from Ref. [33], selecting points from the scan that lie within $\pm 3\sigma$ of all neutrino observables. On the viable obtained points we have imposed the cosmological upper bound on the sum of the masses of the light active neutrinos given by $\sum m_{\nu_i} < 0.12$ eV [82].

Higgs observables

The Higgs sector of the $\mu\nu$ SSM is extended with respect to the (N)MSSM. For constraining the predictions in that sector of the model, we have interfaced HiggsTools [83] with Multinest, using a conservative ± 3 GeV theoretical uncertainty on the SM-like Higgs boson in the $\mu\nu$ SSM as obtained with SPheno. HiggsTools is a unification of HiggsBounds-5 [84–89] and HiggsSignals-2 [90, 91]. Our requirement is that the p-value reported by HiggsTools be larger than 5%, which is equivalent to impose $\chi^2 < 209$ for the 159 relevant degrees of freedom taken into account in our numerical calculation.

• B decays

 $b \to s \gamma$ occurs in the SM at leading order through loop diagrams. We have constrained the effects of new physics on the rate of this process using the average experimental value of BR($b \to s \gamma$) = $(3.55 \pm 0.24) \times 10^{-4}$ provided in Ref. [92]. Similarly to the previous process, $B_s \to \mu^+ \mu^-$ and $B_d \to \mu^+ \mu^-$ occur radiatively. We have used the combined results of LHCb and CMS [93], BR($B_s \to \mu^+ \mu^-$) = $(2.9 \pm 0.7) \times 10^{-9}$ and BR($B_d \to \mu^+ \mu^-$) = $(3.6 \pm 1.6) \times 10^{-10}$. We put $\pm 3\sigma$ cuts from $b \to s \gamma$, $B_s \to \mu^+ \mu^-$ and $B_d \to \mu^+ \mu^-$, as obtained with SPheno. We have also checked that the values obtained are compatible with the $\pm 3\sigma$ of the results from the LHCb collaboration [94], and with the combination of results on the rare $B_s^0 \to \mu^+ + \mu^-$ and $B^0 \to \mu^+ + \mu^-$ decays from the ATLAS, CMS, and LHCb [95].

• $\mu \to e\gamma$ and $\mu \to eee$

We have also included in our analysis the constraints from BR($\mu \to e\gamma$) < 4.2 × 10^{-13} [96] and BR($\mu \to eee$) < 1.0 × 10^{-12} [97], as obtained with SPheno.

• Chargino mass bound

Charginos have been searched at LEP with the result of a lower limit on the lightest chargino mass of 103.5 GeV in RPC MSSM, assuming universal gaugino and sfermion masses at the GUT scale and electron sneutrino mass larger than 300 GeV [98]. This

limit is affected if the mass difference between chargino and neutralino is small, and the lower bound turns out to be in this case 92 GeV [99]. LHC limits can be stronger but for very specific mass relations [100–103]. Although in the $\mu\nu$ SSM there is RPV and therefore these constraints do not apply automatically, we usually choose in our analyses of the model the conservative limit of $m_{\tilde{\chi}_1^\pm} > 92$ GeV. However, since in this work we are analysing the gluino as the LSP, the chargino mass is always well above the mentioned bound.

• Electroweak precision measurements

There have been recently several improvements in EW measurements such as M_W , g-2, S,T,U, etc. (see e.g. Refs. [104–106]). Thus, the confrontation of the theory predictions and experimental results might be timely for SUSY models. We do not impose them in our scans, however, as we will see in Sec. 5, in our framework electroweak precision measurements are not given significant contributions. This is because the SUSY mass spectrum turns out to be above 2.6 TeV, where the latter value is the lower bound that we obtain for the mass of the gluino LSP satisfying the LHC constraints in Sec. 5.

4.2 Parameter Analysis

We performed scans using the minimal possible set of parameters necessary to identify points with the gluino as the LSP. The entire mass spectrum was obtained using the full one-loop numerical computation implemented in SPheno. In what follows, we employed the following steps:

Step 1: The main goal of this step is to find benchmark points satisfying neutrino physics. For this, we started by optimizing the number of parameters of the scan by scanning over the VEVs v_{1L} and v_{2L} and taking the third left sneutrino VEV as $v_{3L} = 1.8 \ v_{2L}$, a relation that is inspired by the specific solution for neutrino physics discussed in Ref. [14]. Also, we scanned over Y_{ν_1} , take $Y_{\nu_2} = 1.8 \ Y_{\nu_1}$ and fix Y_{ν_3} , which allows us to reproduce the normal ordering of neutrino masses with $Y_{\nu_3} < Y_{\nu_1} < Y_{\nu_2}$. Finally, we scanned over the soft bino mass M_1 , which is sufficient to reproduce neutrino data, and fix M_2 .

Concerning Higgs physics, the soft stop masses $m_{\widetilde{Q}_{3L}}$ and $m_{\widetilde{u}_{3R}}$, and the trilinear parameter T_{u_3} are very important for obtaining the correct mass for the SM-like Higgs, as discussed in Sec. 2. In addition, reproducing Higgs data requires suitable additional parameters λ , κ , $\tan \beta$, v_R , T_{κ} and T_{λ} . Nevertheless, we fix κ , T_{κ} and v_R , which basically control the right sneutrino sector, while suitably varying λ , T_{λ} , and $\tan \beta$.

Summarizing, we performed two scans over the 9 parameters discussed above, as shown in Table 1. For Scan 1, the soft mass of the squark doublet is taken as $m_{\widetilde{Q}_{3L}} \in (200, 1200)$ GeV, whereas the soft mass of the right stop is fixed to a large value, $m_{\widetilde{u}_{3R}} = 2000$ GeV, as shown in Table 2. Scan 2 is similar but with the replacement $m_{\widetilde{Q}_{3L}} \leftrightarrow m_{\widetilde{u}_{3R}}$. In Table 2, we also show the remaining benchmark parameters, which are fixed to appropriate values. Note that at this step, the value of M_3 is also fixed according to Table 2.

Step 2: Next, we took advantage of the fact that the parameters controlling neutrino and Higgs physics are essentially decoupled. Of the points derived in *Step 1*, we selected several

Scan 1	Scan 2			
$m_{\tilde{Q}_{3L}} \in (200, 1200)$	$m_{\widetilde{u}_{3R}} \in (200, 1200)$			
$Y_{\nu_1} \in (10^{-8}, 10^{-6})$				
$v_{1,2L} \in (10^{-5}, 10^{-3})$				
$M_1 \in (1500, 2500)$				
$T_{\lambda} \in (0.5, 2000)$				
$\lambda \in (0.3, 0.7)$				
$\tan\beta\in(1,20)$				
$-T_{u_3} \in (0, 2000)$				

Table 1: Range of low-energy values of the input parameters that are varied in the two scans. The VEVs v_{1L}, v_{2L} and the soft SUSY-breaking parameter $m_{\widetilde{Q}_{3L}}, m_{\widetilde{u}_{3R}}, T_{u_3}, M_1$ and T_{λ} are given in GeV. Relations $v_{3L}=1.8\,v_{2L}$ and $Y_{\nu_2}=1.8\,Y_{\nu_1}$ are used.

Scan 1	Scan 2		
$m_{\widetilde{u}_{3R}} = 2000$	$m_{\widetilde{Q}_{3L}} = 2000$		
$\kappa=0.5$			
$-T_{\kappa}=300$			
$Y_{\nu_3} = 10^{-8}$			
$v_R=3500$			
M_2	$M_2=2000,M_3=2700$		
$m_{\widetilde{Q}_{1,2L}} = m_{\widetilde{u}_{1,2R}} = m_{\widetilde{d}_{1,2,3R}} = m_{\widetilde{e}_{1,2,3R}} = 2000$			
$T_{u_{1,2}} = T_{d_{1,2}} = T_{e_{1,2}} = 0$			
$T_{d_3} = 100, T_{e_3} = 40$			
$-T_{\nu_{1,2,3}} = 10^{-3}$			

Table 2: Low-energy values of the input parameters that are fixed in the two scans. The VEV v_R and the soft trilinear parameters, soft wino and gluino masses and soft scalar masses are given in GeV.

starting points for the analysis with fixed values of the parameters that satisfy neutrino physics, namely Y_{ν_1} , v_{1L} , v_{2L} , and M_1 . For these points, we also took the values of Y_{ν_2} and v_{3L} following Table 1, and Y_{ν_3} and M_2 as provided in Table 2. Subsequently, we performed a scan over a subset of the parameters, which are relevant for Higgs physics. Specifically, we varied $m_{\widetilde{Q}_{3L}}$ ($m_{\widetilde{u}_{3R}}$) in the range 900-2000 GeV and $m_{\widetilde{u}_{3R}}$ ($m_{\widetilde{Q}_{3L}}$) in the range 2000-3000 GeV. Additionally, we set the value of T_{u_3} to be as low as -3000 GeV. As for the remaining parameters in Table 1, namely λ , T_{λ} , and $\tan \beta$, we selected specific appropriate values for each of the starting points in the analysis. Furthermore, in order to obtain the gluino as

Scan 3		
$M_3 \in (1900, 3000)$		
$m_{\widetilde{u}_3} \in (1900, 3000)$		
$m_{\widetilde{Q}_3} \in (1900, 3000)$		
$-T_{u_3} \in (0, 5000)$		
$T_{\lambda} \in (0, 4000)$		
$\tan\beta\in(1,10)$		

Table 3: Range of low-energy values of the input parameters that are varied in Scan 3. The soft SUSY-breaking parameters $m_{\widetilde{Q}_{3L}}$, $m_{\widetilde{u}_{3R}}$, T_{u_3} , T_{λ} , and M_3 are given in GeV.

$$\begin{array}{|c|c|c|c|} \mathbf{Scan} \ \mathbf{3} \\ & \lambda = 0.33, \ \kappa = 0.6, \ v_R = 4500 \\ Y_{\nu_1} = 8.82 \times 10^{-7}, \ Y_{\nu_2} = 1.62 \times 10^{-6}, \ Y_{\nu_3} = 4.42 \times 10^{-7} \\ & T_{u_{1,2}} = T_{d_{1,2}} = T_{e_{1,2}} = 0 \\ & T_{d_3} = 100, \ T_{e_3} = 40 \\ & -T_{\nu_{1,2,3}} = 0.1 \\ & -T_{\kappa} = 1200 \\ & m_{\widetilde{Q}_{1,2L}} = m_{\widetilde{u}_{1,2R}} = m_{\widetilde{d}_{1,2,3R}} = m_{\widetilde{e}_{1,2,3R}} = 4500 \ \mathrm{GeV} \\ & M_1 = 3480 \ \mathrm{GeV}, \ M_2 = 3620 \ \mathrm{GeV} \\ \end{array}$$

Table 4: Low-energy values of the input parameters that are fixed in Scan 3. The VEV v_R and the soft trilinear parameters, and soft SUSY-breaking parameters are given in GeV.

the LSP, we varied M_3 in the range of 500-2000 GeV in contrast to Step~1 where it was fixed to a concrete value (see Table 2), and set $T_{\kappa} = -800$ GeV to increase the mass of the pseudoscalar right sneutrinos, and $T_{\nu_{1,2,3}} = -10^{-2}$ GeV to increase the masses of the left sneutrinos and sleptons. Note that with the choice of ranges of different parameters, the stop left (right) is the NLSP in Scan 1 (2).

Step 3: As we will see in the next section, the comparison with LHC data of the results for the points derived from the previous steps, implies that all points found compatible with the experimental constraints of Sec. 4.1, turn out to be excluded. Given this strong constraint, we considered the case of a gluino LSP with a larger mass, namely with soft mass in the range of 1900 - 3000 GeV. The ranges of values of varied parameters, and the values of fixed parameters, are summarized in Tables 3 and 4, respectively.

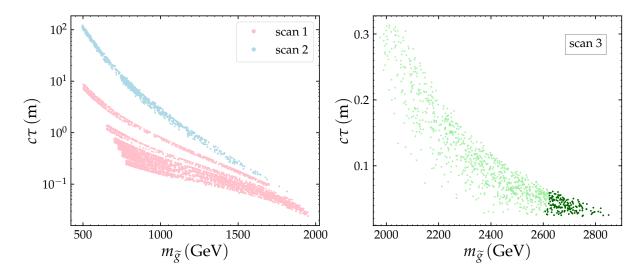


Figure 2: Gluino proper decay length $c\tau$ versus the gluino mass $m_{\tilde{g}}$ for (left plot) Scans 1, 2 shown in Tables 1 and 2, and for (right plot) Scan 3 shown in Tables 3 and 4. All points fulfil the experimental constraints of Sec. 4.1. Cyan, pink and light green points do not fulfil the LHC constraints, while dark green ones do.

5 Results

Following the methods described in the previous sections, in order to find regions consistent with experimental observations we performed scans of the parameter space, and our results are presented here. To carry this analysis out, we selected first points from the scans that lie within $\pm 3\sigma$ of all neutrino physics observables [33]. Second, we put $\pm 3\sigma$ cuts from $b \to s\gamma$, $B_s \to \mu^+\mu^-$ and $B_d \to \mu^+\mu^-$ and require the points to satisfy also the upper limits of $\mu \to e\gamma$ and $\mu \to eee$. In the third step, we imposed that Higgs physics is realized. In particular, we require that the p-value reported by HiggsTools be larger than 5%.

In Fig. 2, we show the decay length of a gluino LSP for the three scans conducted. The left plot pertains to Scans 1 and 2, while the right plot shows the results from Scan 3. As can be seen, all points analysed satisfy the experimental constraints discussed in Sec. 4.1. However, all (pink) points in Scan 1, as well as all (cyan) points in Scan 2, corresponding to gluino masses $m_{\tilde{g}} \lesssim 2000$ GeV, turn out to be excluded because of the LHC constraints discussed in Sec. 3.2. From Case (i), all points with $c\tau > 3m$ and $m_{\tilde{g}} < 2000$ GeV are excluded because of large ionization energy loss. The rest of the points are excluded by the searches for displaced vertices and non-prompt jets corresponding to Cases (ii) to (v).

These results motivated Scan 3, where higher values of $M_3 \lesssim 3000$ GeV were investigated. As can be seen in the right panel, the largest mass of the gluino as the LSP is ~ 2850 GeV, below the upper limit of $M_3 = 3000$ GeV for this scan, since above this value the gluino is no longer the LSP. Constraints from Cases (ii) to (v) exclude the light green points with gluino masses up to $m_{\tilde{g}} \sim 2607$ GeV. Thus, our findings reveal that some regions of the parameter space for the gluino LSP are still compatible with LHC searches, as represented by the dark green points. Note that, the minimum decay length observed is approximately $c\tau \sim 23$ mm for $m_{\tilde{g}} \sim 2850$ GeV, indicating that the prompt decay searches of Case (vi) in Sec. 3.2 are not applicable to our analysis.

In general, the problem to further constrain the lower limit on the gluino mass is that for large masses, the number of predicted events is very scarce (~ 5 events at 137 fb⁻¹ before any selection), and there are simply not enough events to push the limit further, regardless of the analysis. The maximum reachable limit with an ideal search at 13 TeV and 137 fb⁻¹ would be around 2750 GeV actually, where one expects ~ 3 events before selections.

On the other hand, according to Ref. [107], at the HL-LHC, the discovery reach and expected limit of displaced vertex searches in terms of the gluino mass are expected to be improved by ~ 500 GeV and ~ 1000 GeV, respectively, compared to the current limit [39]. Therefore, the remaining points in Fig. 2 can fully be tested in the HL-LHC experiment.

Summarizing, we found that the upper limit for the decay length of the allowed dark green points in the right panel of Fig. 2 is $c\tau \simeq 0.061 \mathrm{m}$, which corresponds to a lower limit on the gluino mass of $m_{\tilde{g}} \simeq 2607$ GeV.

In Fig. 3, the relevant branching ratios (BRs) corresponding to the light and dark green points from the right plot of Fig. 2 (Scan 3) are presented. As anticipated in Sec. 3.1, the dominant decay channels involve third-generation quarks, irrespective of whether neutrinos or leptons are in the final states. In particular, the BR($\tilde{g} \to q\bar{q}'\ell$) constitutes approximately 10% of the BR($\tilde{g} \to t\bar{b}\ell$). Besides, the BR($\tilde{g} \to q\bar{q}\nu$), where q includes the top quark, constitutes approximately 3% of BR($\tilde{g} \to b\bar{b}\nu$). Concerning the latter BRs, it is noteworthy that the BR($\tilde{g} \to t\bar{t}\nu$) is significantly smaller, about 5% of BR($\tilde{g} \to b\bar{b}\nu$). This difference arises because, unlike Eq. (12), the dominant contribution in Eq. (13) is proportional to Y_b . Consequently, for first- and second-generation quarks, where Y_q is negligible, the BR of $\tilde{g} \to q\bar{q}\nu$ (represented as triangles in the upper plot of the left panel) and $\tilde{g} \to t\bar{t}\nu$ are expected to be of similar magnitude.

Additionally, it is worth noting that within the parameter space explored in Scan 3, the BRs exhibit minimal variations. The small differences observed are attributed to variations in the mixing elements between neutrinos and leptons with bino/winos, corresponding to different values of the left neutrino VEVs, v_{iL} . Also, let us remark that the one-loop decay to gluon and neutrino is significantly suppressed and can be considered negligible.

Finally, let us comment that the use of other type of solutions for neutrino physics different from the one presented in Eq. (7), would not modify the results obtained. This can be understood from the summation over leptons present in Eqs. (11-13), since for the most restrictive searches, for instance [38–40], the results are independent of the lepton family or integrate over it. In the particular case of the search [41], where there are muons in the final state, the above conclusion remains valid because the bounds are far from restrictive.

6 Conclusions

We analysed the signals expected at the LHC for a gluino LSP in the framework of the $\mu\nu$ SSM, imposing on the parameter space the experimental constraints on neutrino and Higgs physics, as well as flavour observables such as B and μ decays. The gluino has three relevant decay modes. On the one hand, it has two three-body decays to two quarks and a lepton or a neutrino, mediated by virtual squarks. The dominant channels correspond to the third family of quarks. On the other hand, the gluino can decay to gluon and neutrino

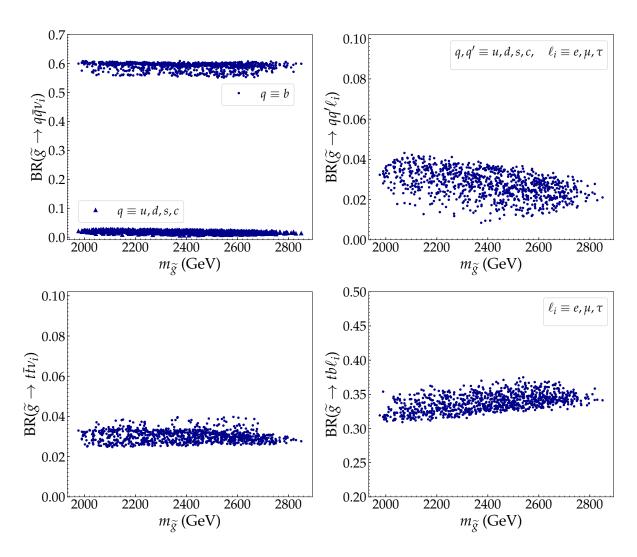


Figure 3: For the points presented in the right panel of Fig. 2, we show the sum of branching ratios of gluino LSP decaying to (left plots) quark-quark-neutrino and (right plots) quark-quark-lepton, versus the gluino mass $m_{\tilde{g}}$. The latter include both the decays into leptons and anti-leptons.

through a virtual quark-squark loop. However, given the large values of the gluino masses analysed, this channel is suppressed compared to the three-body decays. We studied these channels and the corresponding decay lengths for three relevant scans of the parameter space. For two of the scans, we analysed the range for the gluino mass parameter of $M_3 = 500 - 2000$ GeV. We obtained that all points are excluded by the LHC searches of Ref. [36], where a large ionization energy loss is considered. In the third scan, we analysed the wider range of $M_3 = 1900 - 3000$ GeV, obtaining an allowed region. Specifically, searches for displaced vertices and non-prompt jets [38–42] exclude gluino masses up to 2607 GeV, as shown in Fig. 2. Our results also imply an upper limit for the gluino decay length of 6.1 cm.

Acknowledgments

The work of PK and DL was supported by the Argentinian CONICET, and they also acknowledge the support through PICT 2020-02181 The work of EK was supported by the grant "Margarita Salas" for the training of young doctors (CA1/RSUE/2021-00899), co-financed by the Ministry of Universities, the Recovery, Transformation and Resilience Plan, and the Autonomous University of Madrid. The work of IL was funded by the Norwegian Financial Mechanism 2014-2021, grant DEC-2019/34/H/ST2/00707. The research of CM was partially supported by the AEI through the grants IFT Centro de Excelencia Severo Ochoa No CEX2020-001007-S and PID2021-125331NB-I00, funded by MCIN/AEI/10.13039/501100011033. The work of NN was supported by JSPS KAKENHI Grant Number 21K13916.

A Validation of the Search for Displaced Leptons

We tested the implementation of the search using Monte Carlo samples generated for the process $pp \to \tilde{l}^*\tilde{l}$ up to two additional partons in the hard event, where the slepton is either a selectron or smuon and further decays into a neutralino and a electron or muon, respectively. Samples are generated for masses between 50 and 800 GeV and considering proper decay lengths between 3 and 3000 mm. The tree-level sample events are generated with MadGraph5_aMC@NLO-v3.4.2 [72–74] at leading order (LO). Simulated signal events were passed to Pythia-8.306 [77] for parton showering (PS) and hadronization. Jet matching and merging to parton-shower calculations is accomplished by the MLM algorithm [78]. Slepton pair-production nominal cross-sections are derived at NLO using Resummino 3.1.2 [108–114].

Event selection: The event selection utilizes the data provided by the ATLAS collaboration in the auxiliary material. First, it applies a preselection step for truth-level particles, based on a parametrization of the reconstruction and identification efficiency of leptons reported by ATLAS, and requires for the surviving preselected leptons $p_T^l > 65$ GeV and $3 \ mm < |d_0| < 300 \ mm$. Events are then required to have exactly two reconstructed leptons. Then, it applies a parameterized event-level selection based on the acceptance maps reported by ATLAS, as a function of the generator-level p_T of the leading and sub-leading lepton. Additional isolation requirements are placed on the leptons by requiring that the sum of p_T of all tracks that fall within some ΔR of the lepton track are smaller than a fraction f of the lepton- p_T and by requiring that the sum energy deposits near the lepton in the calorimeters must be less than a fraction of the energy of the lepton. Here are the requirements in terms of $(\Delta R, f)$ for the different cases:

- Electrons track: (0.2, 0.06)
- Electrons calorimeter: (0.2, 0.06)
- Muons track: (0.3, 0.04)
- Muons calorimeter: (0.2, 0.15)

Finally, signal leptons are required to be separated by $\Delta R > 0.2$.

Numbers in Tables A.1, A.2 and A.3, and Fig. A.1 show a comparison between the ATLAS results and the recast version of the search. The agreement is generally good but shows a moderately smaller values for lifetimes 0.1-1 ns, coinciding with the largest sensitivity of the search, and shows a larger deviation of the ATLAS sensitivity for values of the lifetime between 0.01-0.1 ns.

Selection	\widetilde{e} (mass [GeV], lifetime [ns])		
	(100, 0.01)	(300, 1)	(500, 0.1)
initial number of events $(\mathcal{L} \times \sigma)$	50830	870	93.6
final selection (ATLAS)	77.1	52.2	17.7
final selection (CheckMATE)	35.0	47.4	10.1
difference [%]	-54.6	-9.3	-43.1

Table A.1: Comparison of the number of expected events in the ee signal region for the process $pp \to \tilde{e}^* \tilde{e}$.

Selection	$\widetilde{\mu}$ (mass [GeV], lifetime [ns])		
	(100, 0.01)	(300, 1)	(500, 0.1)
initial number of events $(\mathcal{L} \times \sigma)$	50830	870	93.6
final selection (ATLAS)	25.0	49.9	13.6
final selection (CheckMATE)	25.33	64.6	10.15
difference [%]	1.3	29.5	-25.4

Table A.2: Comparison of the number of expected events in the $\mu\mu$ signal region for the process $pp \to \widetilde{\mu}^* \widetilde{\mu}$.

Selection	$\widetilde{\tau}$ (mass [GeV], lifetime [ns])	
	(200, 0.1)	(300, 0.1)
initial number of events $(\mathcal{L} \times \sigma)$	4210	870
final selection (ATLAS)	3.45	1.26
final selection (CheckMATE)	2.44	0.55
difference [%]	-41	-56

Table A.3: Comparison of the number of expected events in the $e\mu$ signal region for the process $pp \to \widetilde{\tau}^* \widetilde{\tau}$.

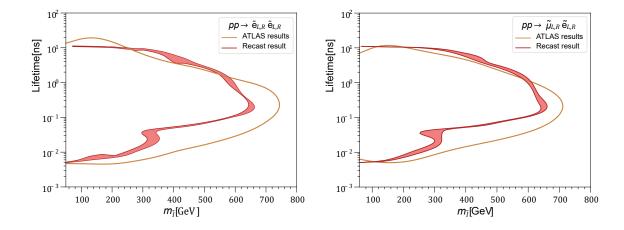
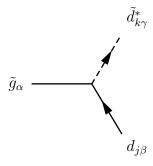


Figure A.1: Comparison of the observed exclusion contours for selectron (smuon) NLSP on the left (right). The orange line shows the ATLAS results and the red line the limit obtained with CheckMATE.

B Gluino LSP Relevant Interactions

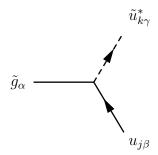
In this Appendix, we write the relevant interactions for our computation of the gluino LSP decays, following SARAH notation [60]. In particular, now a, b = 1, 2, 3 are family indexes, i, j, k are the indexes for the physical states, and $\alpha, \beta, \gamma = 1, 2, 3$ are $SU(3)_C$ indexes $(\alpha = 1, ..., 8)$ when gluinos contribute to the interactions as in (B.1) and (B.2) below, where λ^{α} are the Gell-Mann matrices). The matrices $Z^D, Z^U, U^d_{L,R}, U^u_{L,R}, U^e_{L,R}$ and U^V diagonalize the mass matrices of down squarks, up squarks, down quarks, up quarks, charged fermions (leptons, gauginos and Higgsinos) and neutral fermions (LH and RH neutrinos, gauginos and Higgsinos), respectively. More details about these matrices can be found in Appendix B of Ref. [11]. Taking all this into account, in the basis of 4-component spinors with the projectors $P_{L,R} = (1 \mp \gamma_5)/2$, the interactions for the mass eigenstates are as follows.

B.1 Gluino - down quark - down squark Interaction



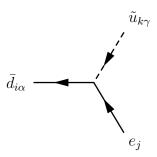
$$-i\frac{1}{\sqrt{2}}g_{3}\lambda_{\gamma,\beta}^{\alpha}\sum_{a=1}^{3}U_{L,ja}^{d,*}Z_{ka}^{D}\left(\frac{1-\gamma_{5}}{2}\right) + i\frac{1}{\sqrt{2}}g_{3}\lambda_{\gamma,\beta}^{\alpha}\sum_{a=1}^{3}Z_{k3+a}^{D}U_{R,ja}^{d}\left(\frac{1+\gamma_{5}}{2}\right)$$
(B.1)

B.2 Gluino - up quark - up squark Interaction



$$-i\frac{1}{\sqrt{2}}g_{3}\lambda_{\gamma,\beta}^{\alpha}\sum_{a=1}^{3}U_{L,ja}^{u,*}Z_{ka}^{U}\left(\frac{1-\gamma_{5}}{2}\right) + i\frac{1}{\sqrt{2}}g_{3}\lambda_{\gamma,\beta}^{\alpha}\sum_{a=1}^{3}Z_{k3+a}^{U}U_{R,ja}^{u}\left(\frac{1+\gamma_{5}}{2}\right)$$
(B.2)

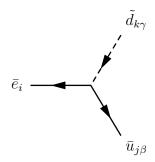
B.3 Up squark - down quark - lepton Interaction



$$i\delta_{\alpha\gamma}U_{R,j5}^{e,*} \sum_{b=1}^{3} Z_{kb}^{U,*} \sum_{a=1}^{3} U_{R,ia}^{d,*} Y_{d,ab} P_{L}$$

$$-i\delta_{\alpha\gamma} \left(g \sum_{a=1}^{3} Z_{ka}^{U,*} U_{L,ia}^{d} U_{L,j4}^{e} - \sum_{b=1}^{3} \sum_{a=1}^{3} Y_{u,ab}^{*} Z_{k3+a}^{U,*} U_{L,ib}^{d} U_{L,j5}^{e}\right) P_{R}.$$
(B.3)

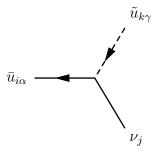
B.4 Down squark - up quark - lepton Interaction



$$i\delta_{\beta\gamma} \left(U_{L,i5}^{e,*} \sum_{b=1}^{3} Z_{kb}^{D,*} \sum_{a=1}^{3} U_{R,ja}^{u,*} Y_{u,ab} \right) P_{L}$$

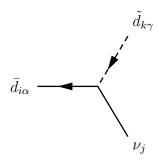
$$- i\delta_{\beta\gamma} \left(g \sum_{a=1}^{3} Z_{ka}^{D,*} U_{L,ja}^{u} U_{R,i4}^{e} - \sum_{b=1}^{3} \sum_{a=1}^{3} Y_{d,ab}^{*} Z_{k3+a}^{D,*} U_{L,jb}^{u} U_{R,i5}^{e} \right) P_{R}.$$
(B.4)

B.5 Up squark - up quark - neutrino Interaction



$$\frac{i}{3}\delta_{\alpha\gamma} \left(2\sqrt{2}g'U_{j4}^{V,*} \sum_{a=1}^{3} Z_{k3+a}^{U,*} U_{R,ia}^{u,*} - 3U_{j7}^{V,*} \sum_{b=1}^{3} Z_{kb}^{U,*} \sum_{a=1}^{3} U_{R,ia}^{u,*} Y_{u,ab}\right) P_{L}
-\frac{i}{6}\delta_{\alpha\gamma} \left[6\sum_{b=1}^{3} \sum_{a=1}^{3} Y_{u,ab}^{*} Z_{k3+a}^{U,*} U_{L,ib}^{u} U_{j7}^{V} + \sqrt{2}\sum_{a=1}^{3} Z_{ka}^{U,*} U_{L,ia}^{u} \left(3gU_{j5}^{V} + g'U_{j4}^{V}\right)\right] P_{R}.$$
(B.5)

B.6 Down squark - down quark - neutrino Interaction



$$-\frac{i}{3}\delta_{\alpha\gamma}\left(\sqrt{2}g'U_{j4}^{V,*}\sum_{a=1}^{3}Z_{k3+a}^{D,*}U_{R,ia}^{d,*}+3U_{j6}^{V,*}\sum_{b=1}^{3}Z_{kb}^{D,*}\sum_{a=1}^{3}U_{R,ia}^{d,*}Y_{d,ab}\right)P_{L}$$

$$-\frac{i}{6}\delta_{\alpha\gamma}\left(6\sum_{b=1}^{3}\sum_{a=1}^{3}Y_{d,ab}^{*}Z_{k3+a}^{D,*}U_{L,ib}^{d}U_{j6}^{V}+\sqrt{2}\sum_{a=1}^{3}Z_{ka}^{D,*}U_{L,ia}^{d}\left(-3gU_{j5}^{V}+g'U_{j4}^{V}\right)\right)P_{R}. \quad (B.6)$$

References

- [1] D. E. López-Fogliani and C. Muñoz, "Proposal for a supersymmetric standard model," *Phys. Rev. Lett.* **97** (2006) 041801, arXiv:hep-ph/0508297 [hep-ph].
- [2] N. Escudero, D. E. López-Fogliani, C. Muñoz, and R. R. de Austri, "Analysis of the parameter space and spectrum of the $\mu\nu$ SSM," *JHEP* **12** (2008) 099, arXiv:0810.1507 [hep-ph].
- [3] D. E. Lopez-Fogliani and C. Munoz, "Searching for Supersymmetry: The $\mu\nu$ SSM (a short review)," Eur. Phys. J. ST **229** no. 21, (2020) 3263-3301, arXiv:2009.01380 [hep-ph].
- [4] H. P. Nilles, "Supersymmetry, Supergravity and Particle Physics," *Phys. Rept.* **110** (1984) 1–162.
- [5] R. Barbieri, "Looking Beyond the Standard Model: The Supersymmetric Option," *Riv. Nuovo Cim.* **11N4** (1988) 1–45.
- [6] H. E. Haber and G. L. Kane, "The Search for Supersymmetry: Probing Physics Beyond the Standard Model," *Phys. Rept.* **117** (1985) 75–263.
- [7] J. Gunion and H. E. Haber, "Higgs Bosons in Supersymmetric Models. 1.," *Nucl. Phys. B* **272** (1986) 1. [Erratum: Nucl.Phys.B 402, 567–569 (1993)].
- [8] S. P. Martin, "A Supersymmetry primer," arXiv:hep-ph/9709356 [hep-ph]. [Adv. Ser. Direct. High Energy Phys.18,1(1998)].
- [9] M. Maniatis, "The Next-to-Minimal Supersymmetric extension of the Standard Model reviewed," Int. J. Mod. Phys. A 25 (2010) 3505-3602, arXiv:0906.0777 [hep-ph].
- [10] U. Ellwanger, C. Hugonie, and A. M. Teixeira, "The Next-to-Minimal Supersymmetric Standard Model," Phys. Rept. 496 (2010) 1–77, arXiv:0910.1785 [hep-ph].
- [11] P. Ghosh, I. Lara, D. E. López-Fogliani, C. Muñoz, and R. Ruiz de Austri, "Searching for left sneutrino LSP at the LHC," Int. J. Mod. Phys. A33 no. 18n19, (2018) 1850110, arXiv:1707.02471 [hep-ph].
- [12] I. Lara, D. E. López-Fogliani, C. Muñoz, N. Nagata, H. Otono, and R. Ruiz De Austri, "Looking for the left sneutrino LSP with displaced-vertex searches," *Phys. Rev.* D98 no. 7, (2018) 075004, arXiv:1804.00067 [hep-ph].
- [13] I. Lara, D. E. López-Fogliani, and C. Muñoz, "Electroweak superpartners scrutinized at the LHC in events with multi-leptons," *Phys. Lett.* **B790** (2019) 176–183, arXiv:1810.12455 [hep-ph].

- [14] E. Kpatcha, I. Lara, D. E. López-Fogliani, C. Muñoz, N. Nagata, H. Otono, and R. Ruiz De Austri, "Sampling the μνSSM for displaced decays of the tau left sneutrino LSP at the LHC," Eur. Phys. J. C 79 no. 11, (2019) 934, arXiv:1907.02092 [hep-ph].
- [15] E. Kpatcha, I. Lara, D. E. López-Fogliani, C. Muñoz, and N. Nagata, "Explaining muon g-2 data in the $\mu\nu$ SSM," Eur. Phys. J. C 81 no. 2, (2021) 154, arXiv:1912.04163 [hep-ph].
- [16] S. Heinemeyer, E. Kpatcha, I. Lara, D. E. López-Fogliani, C. Muñoz, and N. Nagata, "The new $(g-2)_{\mu}$ result and the $\mu\nu$ SSM," Eur. Phys. J. C 81 no. 9, (2021) 802, arXiv:2104.03294 [hep-ph].
- [17] E. Kpatcha, I. Lara, D. E. López-Fogliani, C. Muñoz, N. Nagata, and H. Otono, "Searching for stop LSP at the LHC," Eur. Phys. J. C 82 no. 3, (2022) 261, arXiv:2111.13212 [hep-ph].
- [18] P. Knees, E. Kpatcha, I. Lara, D. E. López-Fogliani, and C. Muñoz, "Searching for sbottom LSP at the LHC," Eur. Phys. J. C 84 no. 1, (2024) 104, arXiv:2309.06456 [hep-ph].
- [19] K.-Y. Choi, D. E. Lopez-Fogliani, C. Muñoz, and R. R. de Austri, "Gamma-ray detection from gravitino dark matter decay in the $\mu\nu$ SSM," JCAP **03** (2010) 028, arXiv:0906.3681 [hep-ph].
- [20] G. A. Gomez-Vargas, M. Fornasa, F. Zandanel, A. J. Cuesta, C. Muñoz, F. Prada, and G. Yepes, "CLUES on Fermi-LAT prospects for the extragalactic detection of μνSSM gravitino dark matter," JCAP 02 (2012) 001, arXiv:1110.3305 [astro-ph.HE].
- [21] A. Albert, G. Gomez-Vargas, M. Grefe, C. Muñoz, C. Weniger, et al., "Search for 100 MeV to 10 GeV γ -ray lines in the Fermi-LAT data and implications for gravitino dark matter in $\mu\nu$ SSM," JCAP 10 (2014) 023, arXiv:1406.3430 [astro-ph.HE].
- [22] G. Gomez-Vargas, D. E. Lopez-Fogliani, C. Muñoz, A. D. Perez, and R. R. de Austri, "Search for sharp and smooth spectral signatures of $\mu\nu$ SSM gravitino dark matter with Fermi-LAT," JCAP 1703 (2017) no.03, 047, arXiv:1608.08640 [hep-ph].
- [23] G. A. Gómez-Vargas, D. E. López-Fogliani, C. Muñoz, and A. D. Perez, "MeV-GeV γ -ray telescopes probing gravitino LSP with coexisting axino NLSP as dark matter in the $\mu\nu$ SSM," Astropart. Phys. **125** (2021) 102506, arXiv:1911.08550 [hep-ph].
- [24] G. A. Gómez-Vargas, D. E. López-Fogliani, C. Muñoz, and A. D. Perez, "MeV-GeV γ -ray telescopes probing axino LSP/gravitino NLSP as dark matter in the $\mu\nu$ SSM," JCAP~2001 no. 01, (2020) 058, arXiv:1911.03191 [hep-ph].
- [25] P. Knees, D. E. Lopez-Fogliani, and C. Muñoz, "Phenomenological implications of sterile neutrinos in the $\mu\nu$ SSM and dark matter," *Astropart. Phys.* **151** (2023) 102865, arXiv:2207.10689 [hep-ph].

- [26] D. J. H. Chung and A. J. Long, "Electroweak Phase Transition in the $\mu\nu$ SSM," *Phys. Rev.* **D81** (2010) 123531, arXiv:1004.0942 [hep-ph].
- [27] Muon g-2 Collaboration, B. Abi et al., "Measurement of the Positive Muon Anomalous Magnetic Moment to 0.46 ppm," Phys. Rev. Lett. 126 no. 14, (2021) 141801, arXiv:2104.03281 [hep-ex].
- [28] Muon g-2 Collaboration, T. Albahri *et al.*, "Measurement of the anomalous precession frequency of the muon in the Fermilab Muon g-2 Experiment," *Phys. Rev. D* 103 no. 7, (2021) 072002, arXiv:2104.03247 [hep-ex].
- [29] T. Aoyama et al., "The anomalous magnetic moment of the muon in the Standard Model," Phys. Rept. 887 (2020) 1–166, arXiv:2006.04822 [hep-ph].
- [30] F. Capozzi, E. Di Valentino, E. Lisi, A. Marrone, A. Melchiorri, and A. Palazzo, "Global constraints on absolute neutrino masses and their ordering," *Phys. Rev.* D95 no. 9, (2017) 096014, arXiv:1703.04471 [hep-ph].
- [31] P. F. de Salas, D. V. Forero, C. A. Ternes, M. Tortola, and J. W. F. Valle, "Status of neutrino oscillations 2018: 3σ hint for normal mass ordering and improved CP sensitivity," *Phys. Lett.* **B782** (2018) 633–640, arXiv:1708.01186 [hep-ph].
- [32] P. F. De Salas, S. Gariazzo, O. Mena, C. A. Ternes, and M. Tórtola, "Neutrino Mass Ordering from Oscillations and Beyond: 2018 Status and Future Prospects," Front. Astron. Space Sci. 5 (2018) 36, arXiv:1806.11051 [hep-ph].
- [33] I. Esteban, M. C. Gonzalez-Garcia, A. Hernandez-Cabezudo, M. Maltoni, and T. Schwetz, "Global analysis of three-flavour neutrino oscillations: synergies and tensions in the determination of θ_{23} , δ_{CP} , and the mass ordering," *JHEP* **01** (2019) 106, arXiv:1811.05487 [hep-ph].
- [34] P. F. de Salas, D. V. Forero, S. Gariazzo, P. Martínez-Miravé, O. Mena, C. A. Ternes, M. Tórtola, and J. W. F. Valle, "2020 global reassessment of the neutrino oscillation picture," *JHEP* **02** (2021) 071, arXiv:2006.11237 [hep-ph].
- [35] I. Esteban, M. C. Gonzalez-Garcia, M. Maltoni, T. Schwetz, and A. Zhou, "The fate of hints: updated global analysis of three-flavor neutrino oscillations," *JHEP* **09** (2020) 178, arXiv:2007.14792 [hep-ph].
- [36] **ATLAS** Collaboration, G. Aad *et al.*, "Search for heavy, long-lived, charged particles with large ionisation energy loss in pp collisions at $\sqrt{s} = 13$ TeV using the ATLAS experiment and the full Run 2 dataset," *JHEP* **2306** (2023) 158, arXiv:2205.06013 [hep-ex].
- [37] **ATLAS** Collaboration, "Search for heavy, long lived charged particles with large specific ionisation and low- β in 140 fb⁻¹ of p p collisions at $\sqrt{s} = 13$ TeV using the ATLAS experiment,".
- [38] CMS Collaboration, A. M. Sirunyan *et al.*, "Search for long-lived particles using nonprompt jets and missing transverse momentum with proton-proton collisions at $\sqrt{s} = 13$ TeV," *Phys. Lett. B* **797** (2019) 134876, arXiv:1906.06441 [hep-ex].

- [39] **ATLAS** Collaboration, M. Aaboud *et al.*, "Search for long-lived, massive particles in events with displaced vertices and missing transverse momentum in $\sqrt{s} = 13$ TeV pp collisions with the ATLAS detector," *Phys. Rev. D* **97** no. 5, (2018) 052012, arXiv:1710.04901 [hep-ex].
- [40] CMS Collaboration, A. M. Sirunyan *et al.*, "Search for long-lived particles using displaced jets in proton-proton collisions at $\sqrt{s} = 13$ TeV," *Phys. Rev. D* **104** no. 1, (2021) 012015, arXiv:2012.01581 [hep-ex].
- [41] **ATLAS** Collaboration, G. Aad *et al.*, "Search for long-lived, massive particles in events with a displaced vertex and a muon with large impact parameter in pp collisions at $\sqrt{s} = 13$ TeV with the ATLAS detector," *Phys. Rev. D* **102** no. 3, (2020) 032006, arXiv:2003.11956 [hep-ex].
- [42] **ATLAS** Collaboration, G. Aad *et al.*, "Search for Displaced Leptons in $\sqrt{s} = 13$ TeV pp Collisions with the ATLAS Detector," *Phys. Rev. Lett.* **127** no. 5, (2021) 051802, arXiv:2011.07812 [hep-ex].
- [43] **ATLAS** Collaboration, G. Aad *et al.*, "Search for R-parity-violating supersymmetry in a final state containing leptons and many jets with the ATLAS experiment using $\sqrt{s} = 13 TeV$ proton-proton collision data," *Eur. Phys. J. C* 81 no. 11, (2021) 1023, arXiv:2106.09609 [hep-ex].
- [44] **ATLAS** Collaboration, G. Aad *et al.*, "Search for pair production of squarks or gluinos decaying via sleptons or weak bosons in final states with two same-sign or three leptons with the ATLAS detector," *JHEP* **02** (2024) 107, arXiv:2307.01094 [hep-ex].
- [45] **CMS** Collaboration, A. Tumasyan *et al.*, "Search for long-lived particles using out-of-time trackless jets in proton-proton collisions at $\sqrt{s} = 13$ TeV," *JHEP* **07** (2023) 210, arXiv:2212.06695 [hep-ex].
- [46] **CMS** Collaboration, A. Hayrapetyan *et al.*, "Search for long-lived particles using displaced vertices and missing transverse momentum in proton-proton collisions at s=13 TeV," *Phys. Rev. D* **109** no. 11, (2024) 112005, arXiv:2402.15804 [hep-ex].
- [47] P. Ghosh and S. Roy, "Neutrino masses and mixing, lightest neutralino decays and a solution to the μ problem in supersymmetry," *JHEP* **04** (2009) 069, arXiv:0812.0084 [hep-ph].
- [48] A. Bartl, M. Hirsch, A. Vicente, S. Liebler, and W. Porod, "LHC phenomenology of the $\mu\nu$ SSM," *JHEP* **05** (2009) 120, arXiv:0903.3596 [hep-ph].
- [49] J. Fidalgo, D. E. López-Fogliani, C. Muñoz, and R. R. de Austri, "Neutrino physics and spontaneous CP violation in the $\mu\nu SSM$," *JHEP* **08** (2009) 105, arXiv:0904.3112 [hep-ph].
- [50] P. Ghosh, P. Dey, B. Mukhopadhyaya, and S. Roy, "Radiative contribution to neutrino masses and mixing in $\mu\nu SSM$," *JHEP* **05** (2010) 087, arXiv:1002.2705 [hep-ph].

- [51] S. Liebler and W. Porod, "On-shell renormalization of neutralino and chargino mass matrices in R-parity violating models - Correlation between LSP decays and neutrino mixing angles revisited," Nucl. Phys. B 855 (2012) 774–800, arXiv:1106.2921 [hep-ph].
- [52] R. Barbier *et al.*, "R-parity violating supersymmetry," *Phys. Rept.* **420** (2005) 1–202, arXiv:hep-ph/0406039 [hep-ph].
- [53] E. Kpatcha, D. E. López-Fogliani, C. Muñoz, and R. Ruiz De Austri, "Impact of Higgs physics on the parameter space of the $\mu\nu$ SSM," Eur. Phys. J. C 80 no. 4, (2020) 336, arXiv:1910.08062 [hep-ph].
- [54] F. Gabbiani, E. Gabrielli, A. Masiero, and L. Silvestrini, "A Complete analysis of FCNC and CP constraints in general SUSY extensions of the standard model," Nucl. Phys. B477 (1996) 321–352, arXiv:hep-ph/9604387 [hep-ph].
- [55] T. Biekotter, S. Heinemeyer, and C. Muñoz, "Precise prediction for the Higgs-boson masses in the $\mu\nu$ SSM," Eur. Phys. J. C78 no. 6, (2018) 504, arXiv:1712.07475 [hep-ph].
- [56] T. Biekotter, S. Heinemeyer, and C. Muñoz, "Precise prediction for the Higgs-Boson masses in the μνSSM with three right-handed neutrino superfields," Eur. Phys. J. C79 no. 8, (2019) 667, arXiv:1906.06173 [hep-ph].
- [57] T. Biekötter, "munuSSM: A python package for the μ -from- ν Supersymmetric Standard Model," Comput. Phys. Commun. **264** (2021) 107935, arXiv:2009.12887 [hep-ph].
- [58] P. Ghosh, D. E. López-Fogliani, V. A. Mitsou, C. Muñoz, and R. Ruiz de Austri, "Probing the μνSSM with light scalars, pseudoscalars and neutralinos from the decay of a SM-like Higgs boson at the LHC," JHEP 11 (2014) 102, arXiv:1410.2070 [hep-ph].
- [59] F. Feroz, M. P. Hobson, and M. Bridges, "MultiNest: an efficient and robust Bayesian inference tool for cosmology and particle physics," Mon. Not. Roy. Astron. Soc. 398 (2009) 1601–1614, arXiv:0809.3437 [astro-ph].
- [60] F. Staub, "SARAH 4: A tool for (not only SUSY) model builders," Comput. Phys. Commun. 185 (2014) 1773, arXiv:1309.7223 [hep-ph].
- [61] W. Porod, "SPheno, a program for calculating supersymmetric spectra, SUSY particle decays and SUSY particle production at e+ e- colliders," *Comput. Phys. Commun.* **153** (2003) 275, arXiv:hep-ph/0301101 [hep-ph].
- [62] W. Porod and F. Staub, "SPheno 3.1: Extensions including flavour, CP-phases and models beyond the MSSM," Comput. Phys. Commun. 183 (2012) 2458–2469, arXiv:1104.1573 [hep-ph].
- [63] Dawson, Sally and Eichten, E. and Quigg, C., "Search for supersymmetric particles in hadron-hadron collisions," Phys. Rev. D 31 (Apr, 1985) 1581–1637.

- [64] W. Beenakker, R. Hopker, M. Spira, and P. M. Zerwas, "Squark and gluino production at hadron colliders," *Nucl. Phys. B* 492 (1997) 51–103, arXiv:hep-ph/9610490.
- [65] W. Beenakker, C. Borschensky, M. Krämer, A. Kulesza, and E. Laenen, "NNLL-fast: predictions for coloured supersymmetric particle production at the LHC with threshold and Coulomb resummation," *JHEP* 12 (2016) 133, arXiv:1607.07741 [hep-ph].
- [66] R. Barbieri, G. Gamberini, G. F. Giudice, and G. Ridolfi, "Constraining Supergravity Models From Gluino Production," Nucl. Phys. B 301 (1988) 15–25.
- [67] S. Chigusa, K. Hamaguchi, T. Moroi, A. Niki, and K. Ono, "Studying squark mass spectrum through gluino decay at 100 TeV future hadron colliders," *Phys. Lett. B* 817 (2021) 136332, arXiv:2102.07910 [hep-ph].
- [68] CheckMATE Collaboration, N. Desai, F. Domingo, J. S. Kim, R. R. d. A. Bazan, K. Rolbiecki, M. Sonawane, and Z. S. Wang, "Constraining electroweak and strongly charged long-lived particles with CheckMATE," Eur. Phys. J. C 81 no. 11, (2021) 968, arXiv:2104.04542 [hep-ph].
- [69] D. Dercks, N. Desai, J. S. Kim, K. Rolbiecki, J. Tattersall, and T. Weber, "CheckMATE 2: From the model to the limit," Comput. Phys. Commun. 221 (2017) 383, arXiv:1611.09856 [hep-ph].
- [70] J. S. Kim, D. Schmeier, J. Tattersall, and K. Rolbiecki, "A framework to create customised LHC analyses within CheckMATE," Comput. Phys. Commun. 196 (2015) 535-562, arXiv:1503.01123 [hep-ph].
- [71] DELPHES 3 Collaboration, J. de Favereau, C. Delaere, P. Demin, A. Giammanco, V. Lemaitre, A. Mertens, and M. Selvaggi, "DELPHES 3, A modular framework for fast simulation of a generic collider experiment," *JHEP* 02 (2014) 057, arXiv:1307.6346 [hep-ex].
- [72] J. Alwall, R. Frederix, S. Frixione, V. Hirschi, F. Maltoni, O. Mattelaer, H. S. Shao, T. Stelzer, P. Torrielli, and M. Zaro, "The automated computation of tree-level and next-to-leading order differential cross sections, and their matching to parton shower simulations," JHEP 07 (2014) 079, arXiv:1405.0301 [hep-ph].
- [73] J. Alwall *et al.*, "Comparative study of various algorithms for the merging of parton showers and matrix elements in hadronic collisions," *Eur. Phys. J. C* **53** (2008) 473–500, arXiv:0706.2569 [hep-ph].
- [74] J. Alwall, S. de Visscher, and F. Maltoni, "QCD radiation in the production of heavy colored particles at the LHC," JHEP 02 (2009) 017, arXiv:0810.5350 [hep-ph].
- [75] R. D. Ball et al., "Parton distributions with LHC data," Nucl. Phys. B 867 (2013) 244-289, arXiv:1207.1303 [hep-ph].

- [76] A. Buckley, J. Ferrando, S. Lloyd, K. Nordstrom, B. Page, M. Rufenacht, M. Schonherr, and G. Watt, "LHAPDF6: parton density access in the LHC precision era," Eur. Phys. J. C75 (2015) 132, arXiv:1412.7420 [hep-ph].
- [77] T. Sjostrand, S. Ask, J. R. Christiansen, R. Corke, N. Desai, P. Ilten, S. Mrenna, S. Prestel, C. O. Rasmussen, and P. Z. Skands, "An introduction to PYTHIA 8.2," Comput. Phys. Commun. 191 (2015) 159–177, arXiv:1410.3012 [hep-ph].
- [78] M. L. Mangano, M. Moretti, F. Piccinini, and M. Treccani, "Matching matrix elements and shower evolution for top-quark production in hadronic collisions," *JHEP* 01 (2007) 013, arXiv:hep-ph/0611129.
- [79] W. Beenakker, M. Kramer, T. Plehn, M. Spira, and P. M. Zerwas, "Stop production at hadron colliders," *Nucl. Phys. B* **515** (1998) 3–14, arXiv:hep-ph/9710451.
- [80] W. Beenakker, S. Brensing, M. Kramer, A. Kulesza, E. Laenen, and I. Niessen, "Supersymmetric top and bottom squark production at hadron colliders," *JHEP* 08 (2010) 098, arXiv:1006.4771 [hep-ph].
- [81] W. Beenakker, C. Borschensky, R. Heger, M. Krämer, A. Kulesza, and E. Laenen, "NNLL resummation for stop pair-production at the LHC," *JHEP* 05 (2016) 153, arXiv:1601.02954 [hep-ph].
- [82] Planck Collaboration, N. Aghanim et al., "Planck 2018 results. VI. Cosmological parameters," Astron. Astrophys. 641 (2020) A6, arXiv:1807.06209 [astro-ph.CO].
- [83] H. Bahl, T. Biekötter, S. Heinemeyer, C. Li, S. Paasch, G. Weiglein, and J. Wittbrodt, "HiggsTools: BSM scalar phenomenology with new versions of HiggsBounds and HiggsSignals," Comput. Phys. Commun. 291 (2023) 108803, arXiv:2210.09332 [hep-ph].
- [84] P. Bechtle, O. Brein, S. Heinemeyer, G. Weiglein, and K. E. Williams, "HiggsBounds: Confronting Arbitrary Higgs Sectors with Exclusion Bounds from LEP and the Tevatron," *Comput. Phys. Commun.* 181 (2010) 138, arXiv:0811.4169 [hep-ph].
- [85] P. Bechtle, O. Brein, S. Heinemeyer, G. Weiglein, and K. E. Williams, "HiggsBounds 2.0.0: Confronting Neutral and Charged Higgs Sector Predictions with Exclusion Bounds from LEP and the Tevatron," Comput. Phys. Commun. 182 (2011) 2605, arXiv:1102.1898 [hep-ph].
- [86] P. Bechtle, O. Brein, S. Heinemeyer, O. Stal, T. Stefaniak, G. Weiglein, and K. E. Williams, "HiggsBounds 4: Improved Tests of Extended Higgs Sectors against Exclusion Bounds from LEP, the Tevatron and the LHC," Eur. Phys. J. C74 no. 3, (2014) 2693, arXiv:1311.0055 [hep-ph].
- [87] P. Bechtle, S. Heinemeyer, O. Stal, T. Stefaniak, and G. Weiglein, "Applying Exclusion Likelihoods from LHC Searches to Extended Higgs Sectors," *Eur. Phys. J.* C75 no. 9, (2015) 421, arXiv:1507.06706 [hep-ph].

- [88] P. Bechtle, D. Dercks, S. Heinemeyer, T. Klingl, T. Stefaniak, G. Weiglein, and J. Wittbrodt, "HiggsBounds-5: Testing Higgs Sectors in the LHC 13 TeV Era," Eur. Phys. J. C 80 no. 12, (2020) 1211, arXiv:2006.06007 [hep-ph].
- [89] H. Bahl, V. M. Lozano, T. Stefaniak, and J. Wittbrodt, "Testing exotic scalars with HiggsBounds," Eur. Phys. J. C 82 no. 7, (2022) 584, arXiv:2109.10366 [hep-ph].
- [90] P. Bechtle, S. Heinemeyer, O. Stal, T. Stefaniak, and G. Weiglein, "HiggsSignals: Confronting arbitrary Higgs sectors with measurements at the Tevatron and the LHC," Eur. Phys. J. C 74 no. 2, (2014) 2711, arXiv:1305.1933 [hep-ph].
- [91] P. Bechtle, S. Heinemeyer, T. Klingl, T. Stefaniak, G. Weiglein, and J. Wittbrodt, "HiggsSignals-2: Probing new physics with precision Higgs measurements in the LHC 13 TeV era," Eur. Phys. J. C 81 no. 2, (2021) 145, arXiv:2012.09197 [hep-ph].
- [92] Heavy Flavor Averaging Group Collaboration, Y. Amhis et al., "Averages of B-Hadron, C-Hadron, and tau-lepton properties as of early 2012," arXiv:1207.1158 [hep-ex].
- [93] **CMS, LHCb** Collaboration, "Combination of results on the rare decays $B_{(s)}^0 \to \mu^+\mu^-$ from the CMS and LHCb experiments, 2013, CMS-PAS-BPH-13-007, LHCb-CONF-2013-012,".
- [94] M. Santimaria, "New results on theoretically clean observables in rare B-meson decays from LHCb," 2021. Talk at LHC Seminar, Mar. 23, 2021.
- [95] **CMS** Collaboration, "Combination of the ATLAS, CMS and LHCb results on the $B^0_{(s)} \to \mu^+\mu^-$ decays, 2020, CMS-PAS-BPH-20-003,".
- [96] **MEG** Collaboration, A. M. Baldini *et al.*, "Search for the lepton flavour violating decay $\mu^+ \to e^+ \gamma$ with the full dataset of the MEG experiment," *Eur. Phys. J. C* **76** no. 8, (2016) 434, arXiv:1605.05081 [hep-ex].
- [97] **SINDRUM** Collaboration, U. Bellgardt *et al.*, "Search for the Decay $\mu^+ \to e^+e^+e^-$," *Nucl. Phys. B* **299** (1988) 1–6.
- [98] "LEP2 SUSY Working Group, ALEPH, DELPHI, L3 and OPAL experiments, note LEPSUSYWG/01-03.1, http://lepsusy.web.cern.ch/lepsusy,".
- [99] "LEP2 SUSY Working Group, ALEPH, DELPHI, L3 and OPAL experiments, note LEPSUSYWG/02-04.1, http://lepsusy.web.cern.ch/lepsusy,".
- [100] **ATLAS** Collaboration, G. Aad *et al.*, "Search for electroweak production of charginos and sleptons decaying into final states with two leptons and missing transverse momentum in $\sqrt{s} = 13$ TeV pp collisions using the ATLAS detector," *Eur. Phys. J. C* **80** no. 2, (2020) 123, arXiv:1908.08215 [hep-ex].

- [101] **CMS** Collaboration, A. M. Sirunyan *et al.*, "Searches for pair production of charginos and top squarks in final states with two oppositely charged leptons in proton-proton collisions at $\sqrt{s} = 13$ TeV," *JHEP* **11** (2018) 079, arXiv:1807.07799 [hep-ex].
- [102] **ATLAS** Collaboration, M. Aaboud *et al.*, "Search for the direct production of charginos and neutralinos in final states with tau leptons in $\sqrt{s} = 13$ TeV pp collisions with the ATLAS detector," *Eur. Phys. J. C* **78** no. 2, (2018) 154, arXiv:1708.07875 [hep-ex].
- [103] **CMS** Collaboration, A. M. Sirunyan *et al.*, "Search for supersymmetry in events with a τ lepton pair and missing transverse momentum in proton-proton collisions at $\sqrt{s} = 13$ TeV," *JHEP* **11** (2018) 151, arXiv:1807.02048 [hep-ex].
- [104] S. Heinemeyer, W. Hollik, D. Stockinger, A. M. Weber, and G. Weiglein, "Precise prediction for M(W) in the MSSM," *JHEP* **08** (2006) 052, arXiv:hep-ph/0604147.
- [105] M. Chakraborti, S. Iwamoto, J. S. Kim, R. Maseλek, and K. Sakurai, "Supersymmetric explanation of the muon g 2 anomaly with and without stable neutralino," *JHEP* 08 (2022) 124, arXiv:2202.12928 [hep-ph].
- [106] G.-C. Cho, K. Hagiwara, Y. Matsumoto, and D. Nomura, "The MSSM confronts the precision electroweak data and the muon g-2," *JHEP* **11** (2011) 068, arXiv:1104.1769 [hep-ph].
- [107] **ATLAS** Collaboration, "Sensitivity of the ATLAS experiment to long-lived particles with a displaced vertex and E_T^{miss} signature at the HL-LHC,".
- [108] J. Debove, B. Fuks, and M. Klasen, "Joint Resummation for Gaugino Pair Production at Hadron Colliders," *Nucl. Phys. B* **849** (2011) 64–79, arXiv:1102.4422 [hep-ph].
- [109] J. Debove, B. Fuks, and M. Klasen, "Transverse-momentum resummation for gaugino-pair production at hadron colliders," *Phys. Lett. B* **688** (2010) 208–211, arXiv:0907.1105 [hep-ph].
- [110] J. Debove, B. Fuks, and M. Klasen, "Threshold resummation for gaugino pair production at hadron colliders," *Nucl. Phys. B* **842** (2011) 51–85, arXiv:1005.2909 [hep-ph].
- [111] B. Fuks, M. Klasen, D. R. Lamprea, and M. Rothering, "Precision predictions for electroweak superpartner production at hadron colliders with Resummino," *Eur. Phys. J. C* **73** (2013) 2480, arXiv:1304.0790 [hep-ph].
- [112] B. Fuks, M. Klasen, D. R. Lamprea, and M. Rothering, "Gaugino production in proton-proton collisions at a center-of-mass energy of 8 TeV," *JHEP* **10** (2012) 081, arXiv:1207.2159 [hep-ph].
- [113] J. Fiaschi and M. Klasen, "Slepton pair production at the LHC in NLO+NLL with resummation-improved parton densities," *JHEP* **03** (2018) 094, arXiv:1801.10357 [hep-ph].

[114] J. Fiaschi and M. Klasen, "Higgsino and gaugino pair production at the LHC with aNNLO+NNLL precision," *Phys. Rev. D* **102** no. 9, (2020) 095021, arXiv:2006.02294 [hep-ph].